Cadasides, calcium-dependent acidic lipopeptides from the soil metagenome that are active against multidrug resistant bacteria

Authors: Changsheng Wu[†], Zhuo Shang[†], Christophe Lemetre, Melinda A. Ternei, Sean F. Brady[*]

[†] These authors contributed equally to this work.

Affiliation: Laboratory of Genetically Encoded Small Molecules, The Rockefeller University, New York, NY 10065.

Corresponding Author (*): Sean F. Brady
Contact: Laboratory of Genetically Encoded Small Molecules, The Rockefeller University
1230 York Avenue, New York, NY 10065
Phone: 212-327-8280
Fax: 212-327-8281
Email: sbrady@rockefeller.edu

Table of contents

Bioassay and labeling methods	Page 4
Supplemental Discussion: Structure determination of cadasides A (**1**) and B (**2**)	Page 7
Table S1. Cadaside biosynthetic gene cluster gene annotations	Page 9
Table S2. ^{1}H and ^{13}C NMR data of cadasides A (**1**) and B (**2**) in CD_3OD	Page 10
Table S3. Retention times (t_R, min) of FDAA derivatives of amino acid (AA) standards and of the hydrolysate of cadaside A (**1**)	Page 12
Table S4. Retention times (t_R, min) for GITC derivatives of L- or D-AMPA standards and of the hydrolysate of cadaside A (**1**)	Page 12
Table S5. Spectrum of activity for cadasides (**1**) and B (**2**)	Page 13
Table S6. List of PCR primers used in this study	Page 14
Figure S1. Phylogenetic tree of AD NPSTs identified by eSNaPD analysis	Page 15
Figure S2. Comparison of the biosynthetic gene clusters for cadasides and other calcium-dependent antibiotics	Page 16
Figure S3. High-resolution mass spectra of cadasides A (**1**) and B (**2**)	Page 17
Figure S4. Structure characterization of cadaside A using 2D NMR correlations	Page 18
Figure S5. ESI-CID-MS/MS fragmentation of cadasides A (**1**) and B (**2**)	Page 19
Figure S6. Annotated ESI-CID-MS/MS fragments of cadaside A (**1**)	Page 20
Figure S7. Key 2D NMR correlations for cadaside B (**2**)	Page 21
Figure S8. Extracted ion chromatogram of L- and D-FDAA derivatives of the hydrolysate of cadaside A (**1**)	Page 22
Figure S9. HPLC-DAD analysis of GITC derivatives of cadaside A hydrolysate and L/D-AMPA standards indicated that the presence of D-AMPA in cadaside A	Page 26
Figure S10. Proposed biosynthetic pathway for cadaside A	Page 27
Figure S11. ^{13}C labelling confirms that the AMPA residue in cadaside originates from thymine.	Page 28
Figure S12. Cadaside A does not depolarize the bacterial cell membrane in a $DiBAC_4$ fluorescence assay	Page 32
Figure S13. Chrome azurol S (CAS) assay for cadaside A, daptomycin and other siderophores	Page 33
Figure S14. ^{1}H NMR (600 MHz, CD_3OD) and UV-vis spectra of cadaside A (**1**)	Page 34
Figure S15. ^{13}C NMR (150 MHz, CD_3OD) spectrum of cadaside A (**1**)	Page 35
Figure S16. ^{1}H-^{13}C HSQC NMR (600 MHz, CD_3OD) spectrum of cadaside A (**1**)	Page 36
Figure S17. ^{1}H-^{13}C HMBC NMR (600 MHz, CD_3OD) spectrum of cadaside A (**1**)	Page 37
Figure S18. ^{1}H-^{1}H COSY NMR (600 MHz, CD_3OD) spectrum of cadaside A (**1**)	Page 38
Figure S19. ^{1}H-^{1}H TOCSY NMR (600 MHz, CD_3OD) spectrum of cadaside A (**1**)	Page 39
Figure S20. ^{1}H-^{13}C HSQC-TOCSY NMR (600 MHz, CD_3OD) spectrum of cadaside A (**1**)	Page 40
Figure S21. ^{1}H-^{1}H ROESY NMR (600 MHz, CD_3OD) spectrum of cadaside A (**1**)	Page 41
Figure S22. ^{1}H NMR (600 MHz, CD_3OD) and UV-vis spectra of cadaside B (**2**)	Page 42
Figure S23. ^{13}C NMR (150 MHz, CD_3OD) spectrum of cadaside B (**2**)	Page 43
Figure S24. ^{1}H-^{13}C HSQC NMR (600 MHz, CD_3OD) spectrum of cadaside B (**2**)	Page 44
Figure S25. ^{1}H-^{13}C HMBC NMR (600 MHz, CD_3OD) spectrum of cadaside B (**2**)	Page 45

Figure S26. ^{1}H-^{1}H COSY NMR (600 MHz, CD_3OD) spectrum of cadaside B (**2**) Page 46
Figure S27. ^{1}H-^{1}H TOCSY NMR (600 MHz, CD_3OD) spectrum of cadaside B (**2**) Page 47
Figure S28. ^{1}H-^{13}C HSQC-TOCSY NMR (600 MHz, CD_3OD) spectrum of cadaside B (**2**) Page 48
Figure S29. ^{1}H-^{1}H ROESY NMR (600 MHz, CD_3OD) spectrum of cadaside B (**2**) Page 49
References Page 50

Bioassay and labeling methods

Microbial susceptibility assays

Cadasides A (**1**) and B (**2**) were assayed in triplicate against 23 bacterial and 3 yeast strains in 96-well microtiter plates using a broth micro-dilution method. Briefly, two-fold serial dilution of **1** and **2** were performed in ddH_2O to make a concentration gradient ranging from 640 to 0.3 μg/mL. Subsequently, 5 μL of each dilution was added to a row of a 96-well microtiter plate followed by supplementing with 5 μL of 1 M $CaCl_2$. For each target microorganism, overnight cultures were diluted 5,000 fold in LB, and 40 μL of the culture dilution was distributed into individual wells. The final test concentration of each compound ranged from 64 to 0.03 μg/mL with a calcium concentration of 100 mM. The microtiter plates were statically incubated at 37 °C for 18 h. The lowest concentration of a compound that inhibits visible growth is recorded as the MIC.

To evaluate the effect of calcium on cadaside activity, a bacterial susceptibility assay using **1** was performed on *S. aureus* NRS100 in the presence of $CaCl_2$ ranging from 400 mM to 6.25 mM (two-fold serial dilutions). The dose-response curve was plotted using GraphPad Prism 7.0 software (La Jolla, CA). MICs of tetracycline, ampicillin, chloramphenicol, rifamycin, vancomycin, kanamycin and daptomycin were also evaluated by the broth micro-dilution method using *S. aureus* NRS100 and *E. faecium* ATCC 51559 in the presence and absence of 100 mM $CaCl_2$. To test the ability of other metal ions to promote cadaside antibiosis, bacterial susceptibility assays of **1** against *S. aureus* NRS100 were performed by supplementing different monovalent (NaCl and KCl), divalent ($CaCl_2$, $MgCl_2$, $BaCl_2$, $SrCl_2$, $ZnSO_4$, $FeSO_4$, $MnCl_2$, $CuCl_2$ and $CdCl_2$) and trivalent ($FeCl_3$ and $AuCl_3$) metal ions. We assessed the toxicity of these metal ions alone and then performed cadaside susceptibility assays in the presence of the metals at one quarter of their MIC. In all of our microbial susceptibility assays, calcium chloride was added to autoclaved LB broth as a sterile filtered stock solution.

Cytotoxicity assay

The cytotoxicity of cadasides A (**1**) and B (**2**) were tested on HeLa, HT29 and NCI-H1299 cells using the MTT (3-(4,5-dimethylthiazol-2-yl)-2,5-diphenyltetrazolium bromide) assay.[1] Briefly, tested cells (2,500 cells/well) were seeded in a 96-well microtiter plate and incubated in DMEM (HeLa, HT29) and RPMI 1640 (NCI-H1299) media (with 10% fetal bovine serum) at 37 °C for 24 h with 5% CO_2. Cadasides A (**1**) and B (**2**) were added to each well at final concentrations ranging from 128 to 0.5 μg/mL. After a 48 h incubation, the media was removed from each well and 110 μL of MTT solution (10 μL of 5 mg/mL MTT in PBS premixed with 100 μL of DMEM or RPMI 1640) was added. After a 3 h incubation at 37 °C with 5% CO_2, the solution was aspirated and precipitated formazan crystals were dissolved by addition of 100 μL of solubilization solution (40% DMF, 16% SDS and 2% acetic acid in H_2O). The absorbance of each well was measured at OD_{570} using a microplate reader (Epoch Microplate Spectrophotometer, BioTek). Taxol was used as the positive control. IC_{50} values were calculated (Prism 7.0) as the concentration of each compound required for 50% inhibition of cell growth relative to the no compound controls. All experiments were performed in triplicate.

Membrane leakage and depolarization assays

The effect of cadaside A (**1**) on bacterial cell membrane permeability was evaluated using SYTOX green nucleic acid stain (Thermo Fisher). Briefly, 900 μL of *S. aureus* NRS100 LB culture (OD_{600} = 0.35) either supplemented with or without 100 mM $CaCl_2$ was mixed with 100 μL of SYTOX green (17 μM in DMSO).

Each mixture was kept at room temperature for 5 min, and then distributed into 96-well microtiter plates at 50 µL per well. The initial fluorescence readout of each well was recorded using a SpectraMax M2 (Molecular Devices) with excitation and emission wavelengths at 488 nm and 523 nm, respectively. 50 µL of each test compound [cadaside A, daptomycin (positive control) and vancomycin (negative control)] was added to sets of three wells (final concentration 50 µg/mL). The fluorescence of each well was then monitored every 9 seconds for 20 min.

Bacterial cell membrane depolarization assays were conducted in a similar manner as the membrane lysis assays. In short, 900 µL of *S. aureus* NRS100 LB culture (OD_{600} = 0.35) supplemented either with or without 100 mM $CaCl_2$ was mixed with 100 µL of $DiBAC_4(3)$ (bis-(1,3-dibutylbarbituric acid)trimethine oxonol) dye (Thermo Fisher, 20 µg/mL in DMSO). The resulting mixtures were incubated at room temperature for 5 min before distribution into 96-well microtiter plates at 50 µL per well. The initial fluorescence was acquired with excitation and emission wavelengths at 490 nm and 516 nm, respectively. 50 µL of each test compound [cadaside A, daptomycin (positive control) and vancomycin (negative control)] was subsequently added to sets of three wells (final concentration 50 µg/mL). The fluorescence of each well was then monitored at every 9 seconds for 20 min.

UDP-MurNAc-pentapeptide accumulation assay

The effect of cadaside A (**1**) on *S. aureus* NRS100 cell wall biosynthesis was assessed by looking for the accumulation of the peptidoglycan nucleotide precursor UDP-MurNAc-pentapeptide.[2] Briefly, LB cultures of *S. aureus* NRS100 were grown either with or without 100 mM $CaCl_2$ to an OD_{600} of 0.6 and then treated with chloramphenicol at a final concentration of 130 µg/mL. After a 15 min incubation at 37 °C, 200 µL aliquots of bacterial culture were distributed into 1.7 mL Eppendorf tubes. Antibiotics were then added to approximately 10 × their MIC (50 µg/mL for cadaside A, 2.5 µg/mL for daptomycin and 20 µg/mL for vancomycin). After 60 min of shaking (250 rpm) at 37 °C, bacterial cells were collected by centrifugation at 3,200 ×*g* and then resuspended in 30 µL of ddH_2O. The suspension was boiled for 15 min after which insoluble cell debris was removed by centrifuge. The resulting supernatant was analyzed by UPLC-DAD-MS (Acquity UPLC BEH C_{18}, 2.1 × 50 mm, 1.7 µm, 130 Å, 0.77 mL/min isocratic elution at 98% H_2O/MeCN for 2 min, then from 98% to 20% H_2O/MeCN over 1.4 min, with constant 0.1% formic acid; positive and negative ionization modes). Using masses of 1150 $[M + H]^+$ or 1148 $[M - H]^-$, the presence of UDP-MurNAc-pentapeptide was tracked in the total ion chromatograms generated in these analyses.

Chrome azurol S (CAS) assay

The iron binding ability of the cadasides was measured using the CAS assay.[3,4] Briefly, 7.5 mL of 2 mM aqueous CAS solution and 1.5 mL of 1 mM $FeCl_3$ solution (prepared in 10 mM HCl) were added to 25 mL of hexadecyltrimethylammonium bromide (CTAB) solution (0.876 mg/mL). This CAS-Fe(III)-CTAB solution was mixed with 50 mL of 2-(*N*-morpholino)ethanesulfonic acid (MES) buffer (195.2 mg/mL, pH 5.6) and ddH_2O was used to adjust the final volume to 100 mL. For the CAS assay, 50 µL of the assay solution was distributed into a 96-well microtiter plate. Two-fold serial dilutions of cadaside A (**1**) as well as the known iron chelators deferoxamine mesylate, pyoverdines, iron-free ferrichrome, disodium EDTA, and citric acid were prepared in ddH_2O. 50 µL of these dilution series were added to distinct microtiter plate wells to give final concentrations

ranging from 1.28 mM to 1.25 μM. After incubation at 37 °C for 3 h, the color change in each well was measured at 630 nm.

$^{13}CH_3$-thymine labelling

S. albus J1074 containing BAC-DFD0097-157/431/2621 was inoculated into 1 mL of R5A broth supplemented with 3.5 mg of $^{13}CH_3$-thymine in a 24-well Micro-Flask (Applikon Biotechnology). A culture supplemented with the same amount of unlabeled thymine was used as the negative control. Eight-day old cultures (250 rpm, 30 °C) were extracted with HP-20 resin and the resin was subsequently eluted by methanol. The methanol eluate was dried *in vacuo* and the extract was dissolved in 50 μL of 50% aqueous methanol. HPLC-HRMS-MS/MS analysis was performed on a Thermo Scientific LTQ Orbitrap XL Hybrid Ion Trap-Orbitrap Mass Spectrometer connected to a Dionex UltiMate 3000 HPLC system. The HPLC condition was set as follows: Thermo Acclaim 120 RP-C_{18} column, 2.1 × 150 mm, 5 μm, 0.2 mL/min gradient elution from 95% to 40% H_2O/MeCN over 20 min, then 100% MeCN for 5 min, and finally 95% H_2O/MeOH for 5 min, with constant 0.1% formic acid. The ESI source parameters were set as follows: capillary temperature 350 °C, sheath gas flow 8 units, positive polarity, and source voltage 4.0 kV. For the targeted CID-FT MS-MS spectra, the peak containing a single ^{13}C atom (*m/z* 780.34) among the $[M + 2H]^{2+}$ isotope peak cluster for cadaside A (**1**) was selected for fragmentation under a normalized collision energy of 35%. The enrichment of isotope peaks was analyzed using Thermo Xcalibur 2.0.7 software and the ratios were calculated manually.

Structure determination of cadasides A (1) and B (2)

Cadaside A (**1**, 8.5 mg) was isolated as a brown powder from *S. albus*-BAC-DFD0097-157/431/262 R5A culture broth (25 L). HPLC-HRESI(+)MS analysis of **1** returned a protonated ion at *m/z* 1558.6796 $[M + H]^+$ (calcd for $C_{69}H_{100}N_{13}O_{28}^+$, 1558.6795), suggesting a molecular formula of $C_{69}H_{99}N_{13}O_{28}$ (Figure S2). 2D NMR (COSY, TOCSY, HSQC, HMBC, and HSQC-TOCSY) analyses revealed that cadaside A is comprised of an unsaturated fatty acid chain and 13 amino acid residues (Figure S3, A). The lipid chain was determined to be 8-methyldeca-2,4-dienoic acid (MDDA) with two conjugated double bonds at *cis*-Δ^2 and *trans*-Δ^4 on the basis of diagnostic coupling constants ($J_{2,3}$ = 11.4 Hz and $J_{4,5}$ = 15.3 Hz) and NOE correlations between H-2/H-3 and H-3/H-5 (Figure S3, B). The 13 amino acid residues in **1** were characterized as 3-amino-2-methylpropionic acid (AMPA), glycine (2 × Gly), glutamic acid (2 × Glu), tyrosine (Tyr), threonine (Thr), isoleucine (Ile), aspartic acid (Asp), β-hydroxyaspartic acid (β-hyAsp), proline (Pro), 4-hydroxy-glutamic acid (γ-hyGlu), and sarcosine (Sar) (Figure S3, B). The rare AMPA residue was first suggested by a COSY/TOCSY spin system consisting of a methyl doublet at δ_H 1.14 (d, J = 6.9 Hz, H_3-4), a methine at δ_H 2.66 (m, H-2), and a *N*-bearing inequivalent methylene at δ_H 3.26 (dd, J = 13.4, 8.4 Hz, H-3a) and δ_H 3.43 (dd, J = 13.4, 5.7 Hz, H-3b). The HMBC correlations from H_3-4 to C-3 (δ_C 43.6) and the amide carbonyl group (δ_C 178.2) further supported the presence of an AMPA residue. The hydroxyl group on the hyGlu residue was located at the C-4 (δ_C 69.1) based on sequential COSY correlations from δ_H 5.14 (H-2) to δ_H 1.93/2.30 (H_2-3) then to δ_H 4.16 (H-2). The assignments of ^{1}H and ^{13}C NMR data of the lipid chain and each amino acid residue in **1** and **2** were summarized in Table S2.

The amino acid sequences of **1** and **2** were first predicted by bioinformatics, and then established conclusively by 2D NMR and tandem mass spectrometry. Specifically, three large structural pieces of **1**, including MDDA-$AMPA_1$-Gly_2, Glu_3-Tyr_4-Thr_5-Ile_6, and Pro_9-Gly_{10}-Glu_{11}-γ-hyGlu_{12}-Sar_{13} were built by inspecting HMBC correlations from α protons to carbonyl carbon of the previous amino acid residue (Figure S3, B). The connection between γ-hyGlu_{12} and Sar_{13} was demonstrated by the HMBC correlation from *N*-CH_3 to the carbonyl carbon of γ-hyGlu_{12} as well as a ROESY cross peak between *N*-CH_3 and H-2/H-3 of γ-hyGlu_{12} (Figure S3, B). Due to the lack of inter-residue HMBC signals for Asp_7 and β-hyAsp_8, their connections to other amino acid residues remained uncertain at that stage. Cde NRPSs contain a total of 13 adenylation (AD) domains, perfectly matching the 13 amino acids analytically predicted to be present in the cadasides (Figure S9). The bioinformatic analysis of AD domain specificities indicated a predicted peptide sequence of: lipid-X_1-Gly_2-Asp_3-Tyr_4-Thr_5-Val_6-Asp_7-Asp_8-Pro_9-Gly_{10}-Asp_{11}-Asp_{12}-Sar_{13}. By comparing this theoretical peptide sequence with the experimentally NMR-resolved partial structures we connected the five established structural pieces (Figure S3, B) and proposed a lipidated peptide sequence of: MDDA-$AMPA_1$-Gly_2-Glu_3-Tyr_4-Thr_5-Ile_6-Asp_7-β-hyAsp_8-Pro_9-Gly_{10}-Glu_{11}-γ-hyGlu_{12}-Sar_{13}. To further corroborate this deduced structure, an ESI-MS/MS experiment was conducted to generate the peptide fragment ions of **1** (Figure S4). The structural annotation of observed fragment ion pairs is elaborated in Figure S5. Fragment ion pairs that were critical to unambiguously elucidate the planar structure of cadaside A (**1**) were as follows. Collision-induced dissociation (CID) fragmentation of the selected precursor ion 779.84 $[M + 2H]^{2+}$ afforded a set of complementary ion pairs (*m/z* 250/1309, *m/z* 307/1252, *m/z* 436/1123 and *m/z* 599/960 (Figure S5) that allowed us to unequivocally define the following substructure: MDDA-$AMPA_1$-Gly_2-Glu_3-Tyr_4. Three additional pairs of fragment ions, *m/z* 884/675, *m/z* 999/560, *m/z* 1130/429, not only demonstrated the linkage of Ile_6-Asp_7-β-hyAsp_8-Pro_9, but also revealed the ring closure between Thr_5 and Sar_{13} through an ester bond.

Cadaside B (**2**, 5.0 mg) was co-isolated with cadaside A. HPLC-HRESI(+)MS analysis of **2** revealed a protonated ion at *m/z* 1544.6633 $[M + H]^+$ (calcd for $C_{68}H_{98}N_{13}O_{28}^+$, 1544.6639), which is indicative of the loss of CH_2 compared to **1**. Analysis of the MS/MS data from **1** and **2** (Figure S4) revealed this difference was located in the lipid chain. Detailed inspection of 1D and 2D NMR data (Table S2) permitted the assignment of the lipid in cadaside B (**2**) as (2*Z*,4*E*)-8-methylnona-2,4-dienoic acid (MNDA). By comparison of NMR and MS/MS data the peptide substructure of **2** proved to be identical to that of **1**. Therefore, the planar structure of cadaside B (**2**) was assigned as shown in Figure S6.

The absolute configurations of the amino acid residues in **1** and **2** were determined by chemical derivatization with 1-fluoro-2,4-dinitrophenyl-5-L-alanine amide (L-FDAA), 1-fluoro-2,4-dinitrophenyl-5-D-alanine amide (D-FDAA), and 2,3,4,6-tetra-*O*-acetyl-*β*-D-glucopyranosyl isothiocyanate (GITC). Through the comparison of retention times of L-FDAA and D-FDAA derivatives of cadaside hydrolysate with those of amino acid standards, we elucidated the absolute configuration of each amino acid residue as shown in Table S3. Specifically, Glu_3, Glu_{11} and Ile_6 were assigned to be D-amino acids, while Tyr_4, Thr_5, Asp_7, β-$hyAsp_8$, Pro_9 and γ-$hyGlu_{12}$ were found to be in L-configurations. The β-CH in β-$hyAsp_8$ and γ-CH in γ-$hyGlu_{12}$ were also determined to be *R* by comparison with FDAA derivatives of amino acid standards (Figure S8). However, L- and D-FDAA derivatives of AMPA could not be resolved under our column and elution conditions, therefore we sought to use GITC to derivatize AMPA. HPLC profile comparison of GITC derivatives of cadaside hydrolysate with those of L- and D-AMPA standards indicated the presence of D-AMPA in the cadasides (Table S4 and Figure S8).

Table S1. Cadaside biosynthetic gene cluster gene annotations (GeneBank Accession NO. MK060022).[a]

ORF	Gene size (bp)	Gene name	Proposed function	NCBI similarity	ID%
1	1266	*cdeA*	AMPA biosynthesis	cytochrome P450 [*Streptomyces rhizosphaericus*]; WP_086884385.1	85%
2	807	*cdeB*	AMPA biosynthesis	alpha/beta hydrolase [*Streptomyces rhizosphaericus*]; WP_086884384.1	86%
3	849	*cdeC*	Transport	ABC transporter permease [*Streptomyces rhizosphaericus*]; WP_086884383.1	76%
4	939	*cdeD*	Transport	daunorubicin/doxorubicin resistance ABC transporter ATP-binding protein DrrA [*Streptomyces rhizosphaericus*]; WP_086884382.1	76%
5	1761	*cdeE*	Acyl-CoA/AMP synthesis	acyl-CoA synthase [uncultured bacterium esnapd2]; WP_086884379.1	74%
6	1704	*cdeF*	Desaturation of acyl chain	acyl-CoA dehydrogenase [*Streptomyces* sp. MBT76]; WP_107105521.1	69%
7	1737	*cdeG*	Desaturation of acyl chain	acyl-CoA dehydrogenase [*Streptomyces glaucescens*]; WP_086732724.1	71%
8	291	*cdeH*	Attachment of acyl chain	acyl carrier protein [*Streptomyces rhizosphaericus*]; WP_086884377.1	70%
9	21714	*cdeI*	NRPS	non-ribosomal peptide synthetase [*Streptomyces ambofaciens*]; WP_079030454.1	51%
10	17127	*cdeJ*	NRPS	non-ribosomal peptide synthetase [*Streptomyces ambofaciens*]; WP_079155636.1	51%
11	8355	*cdeK*	NRPS	non-ribosomal peptide synthetase [*Streptomyces* sp. CB02923] WP_073766514.1	50%
12	222	*cdeL*	Unknown	mbtH-like protein [*Streptomyces varsoviensis*]; KOG43121.1	83%
13	732	*cdeM*	Unknown	phosphatase PAP2 family protein [*Streptomyces rhizosphaericus*]; WP_086879388.1	68%
14	975	*cdeN*	Hydroxylation of Asp and Glu	alpha-ketoglutarate-dependent taurine dioxygenase [*Plantactinospora* sp. CNZ320]; PKV26967.1	69%
15	1062	*cdeO*	D-Ile biosynthesis	branched-chain amino acid aminotransferase [*Streptomyces rhizosphaericus*]; WP_086879374.1	76%
16	387	*cdeP*	D-Ile biosynthesis	ketosteroid isomerase [*Streptomyces* sp. DvalAA-43]; WP_093539559.1	65%
17	696	*cdeQ*	Unknown	phosphatase PAP2 family protein [*Streptomyces rhizosphaericus*]; WP_086879389.1	69%
18	1455	*cdeR*	Regulation	sensor histidine kinase [*Streptomyces* sp. MH60]; WP_104633320.1	64%
19	639	*cdeS*	Regulation	DNA-binding response regulator [*Streptomyces rhizosphaericus*]; WP_086879390.1	85%
20	1131	*cdeT*	AMPA biosynthesis	succinate-semialdehyde dehydrogenase [*Streptomyces scopuliridis* RB72]; PVE07583.1	76%

[a] The upstream boundary of *cde* gene cluster was conservatively defined as being the gene directly adjacent to another NRPS system upstream of the *cde* NRPS genes. This second set of NRPS genes is not closely related to genes found in any calcium-dependent antibiotic biosynthetic gene cluster. The downstream edge of the *cde* cluster was defined by the appearance of genes predicted to be involved in primary metabolism instead of secondary metabolism.

Table S2. ^{1}H and ^{13}C NMR data of cadasides A (**1**) and B (**2**) in CD_3OD

Pos.	**cadaside A (1)**		**cadaside B (2)**	
	δ_C, type	δ_H, mult. (*J* in Hz)	δ_C, type	δ_H, mult. (*J* in Hz)
	8-methyldeca-2,4-dienoic acid (MDDA)		**8-methylnona-2,4-dienoic acid (MNDA)**	
1	169.3, C	–	169.3, C	–
2	119.4, CH	5.62, d (11.4)	119.4, CH	5.62, d (11.3)
3	143.0, CH	6.40, t (11.4)	143.0, CH	6.40, t (11.3)
4	128.3, CH	7.41, dd (15.3, 11.4)	128.4, CH	7.41, dd (15.3, 11.3)
5	144.7, CH	5.99, d (15.3, 7.0)	144.6, CH	5.99, d (15.3, 7.0)
6	31.4, CH_2	2.16; 2.21	31.9, CH_2	2.16; 2.21
7	36.9, CH_2	1.26; 1.47	39.3, CH_2	1.33, m
8	35.3, CH	1.37	28.8, CH	1.58, m
9	11.7, CH_3	0.88	22.8, CH_3	0.91
10	30.4, CH_2	1.18; 1.37	22.8, CH_3	0.91
11	19.4, CH_3	0.89	–	–
	AMPA-1		**AMPA-1**	
1	178.2, C	–	178.2, C	–
2	41.9, CH	2.66, m	41.9, CH	2.66, m
3	43.6, CH_2	3.26, dd (13.4, 8.4); 3.43, dd (13.4, 5.7)	43.6, CH_2	3.26, dd (13.4, 8.4); 3.42, dd (13.4, 5.7)
4	15.7, CH_3	1.14, d (6.9)	15.7, CH_3	1.14, d (6.9)
	Gly-2		**Gly-2**	
1	171.6, C	–	171.6, C	–
2	43.9, CH_2	3.80, d (16.5); 3.94, d (16.5)	43.9, CH_2	3.79, d (16.6); 3.93, d (16.6)
	Glu-3		**Glu-3**	
1	174.2, C	–	174.0, C	–
2	54.9, CH	4.33	54.8, CH	4.33
3	27.9, CH_2	2.15	27.9, CH_2	2.15
4	31.6, CH_2	2.38, dt (16.4, 7.8); 2.49, dt (16.4, 7.1)	31.5, CH_2	2.38, dt (16.6, 7.9); 2.48, dt (16.6, 7.2)
5	176.8, C	–	176.8, C	–
	Tyr-4		**Tyr-4**	
1	174.4, C	–	174.4, C	–
2	56.5, CH	4.76, br s	56.5, CH	4.75, br s
3	37.8, CH_2	2.91; 3.18	37.8, CH_2	2.91; 3.18
4	129.0, C	–	129.0, C	–
5/9	131.4, CH	7.10, d (8.1)	131.4, CH	7.10, d (8.1)
6/8	116.4, CH	6.70, d (8.1)	116.4, CH	6.70, d (8.1)
7	157.4, C	–	157.4, C	–
	Thr-5		**Thr-5**	
1	171.2, C	–	171.3, C	–
2	58.7, CH	4.58, br s	58.6, CH	4.58, br s
3	71.8, CH	5.50, br s	71.7, CH	5.51, br s
4	17.1, CH_3	1.28, d (6.6)	17.2, CH_3	1.27, d (6.5)
	Ile-6		**Ile-6**	
1	173.0, C	–	173.0, C	–
2	59.2, CH	4.27, d (6.9)	59.2, CH	4.25, d (6.9)
3	38.1, CH	1.87	38.1, CH	1.87
4	26.0, CH_2	1.13; 1.52	26.0, CH_2	1.14; 1.52

5	11.7, CH_3	0.89	11.7, CH_3	0.89
6	15.8, CH_3	0.93, d (6.9)	15.8, CH_3	0.93
	Asp-7		**Asp-7**	
1	172.5, C	–	172.6, C	–
2	51.2, CH	5.01, br s	51.2, CH	4.99, br s
3	36.9, CH_2	2.70; 2.88	36.9, CH_2	2.71; 2.87
4	174.2, C	–	174.4, C	–
	β-HyAsp-8		**β-HyAsp-8**	
1	171.5, C	–	171.5, C	–
2	74.0, CH	4.38, d (4.4)	74.1, CH	4.36, d (4.4)
3	55.5, CH	4.95	55.6, CH	4.93
4	177.1, C	–	177.1, C	–
	Pro-9		**Pro-9**	
1	174.9, C	–	174.9, C	–
2	63.5, CH	4.30	63.5, CH	4.30
3	30.4, CH_2	1.83; 2.21	30.4, CH_2	1.82; 2.21
4	26.3, CH_2	1.90; 2.01, m	26.3, CH_2	1.88, m; 2.00, m
5	49.3, CH_2	3.79; 3.95	49.3, CH_2	3.77; 3.95
	Gly-10		**Gly-10**	
1	172.5, C	–	172.5, C	–
2	43.3, CH_2	3.71, d (16.9); 4.18, d (16.9)	43.3, CH_2	3.70, d (17.1); 4.18, d (17.1)
	Glu-11		**Glu-11**	
1	173.5, C	–	173.5, C	–
2	53.9, CH	4.47, br s	53.9, CH	4.47, br s
3	28.6, CH_2	1.80; 2.00	28.7, CH_2	1.80; 2.01
4	31.0, CH_2	2.16; 2.21	31.1, CH_2	2.16; 2.21
5	176.6, C	–	176.7, C	–
	γ-HyGlu-12		**γ-HyGlu-12**	
1	173.9, C	–	174.0, C	–
2	47.7, CH	5.14, br s	47.8, CH	5.12, br s
3	37.4, CH_2	1.93; 2.30, m	37.4, CH_2	1.93; 2.30, m
4	69.1, CH	4.16	69.4, CH	4.12, br s
5	178.2, C	–	178.4, C	–
	Sar-13		**Sar-13**	
1	169.7, C	–	169.7, C	–
2	51.2, CH_2	3.64, d (16.9); 4.67, d (16.9)	51.2, CH_2	3.62, d (16.3); 4.67, d (16.3)
N-CH_3	37.3, CH_3	3.22, s	37.4, CH_3	3.22, s

^{1}H and ^{13}C NMR were obtained at 600 and 150 MHz, respectively. The assignments of overlapping ^{1}H NMR signals were supported by HSQC, HMBC, TOCSY and HSQC-TOCSY. The peak multiplicity and coupling constants are presented for non-overlapping signals only.

Table S3. Retention times (t_R, min) of FDAA derivatives of amino acid (AA) standards and of the hydrolysate of cadaside A (**1**)

AA	MW	AA standards		hydrolysate of **1**		
		$t_{R\ (L\text{-}AA\text{-}L\text{-}FDAA)}$ or $t_{R\ (D\text{-}AA\text{-}D\text{-}FDAA)}$ (min)	$t_{R\ (L\text{-}AA\text{-}D\text{-}FDAA)}$ or $t_{R\ (D\text{-}AA\text{-}L\text{-}FDAA)}$ (min)	$t_{R\ (AA\text{-}L\text{-}FDAA)}$ (min)	$t_{R\ (AA\text{-}D\text{-}FDAA)}$ (min)	L or D
AMPA	355	16.60	16.60	16.60	16.60	NA
Glu	399	11.39	13.16	13.20	11.42	D
Tyr	433	17.06	19.49	17.11	19.52	L
Thr	371	9.32	13.45	9.41	13.43	L
allo-Thr	371	9.61	11.27	–	–	–
Ile	383	23.80	28.59	28.59	23.80	D
allo-Ile	383	23.80	28.59	–	–	–
Asp	385	9.67	11.05	9.78	11.03	L
Pro	367	14.49	15.97	14.56	15.98	L
β-hyAsp	401	8.28 (2*S*, 3*R*, $_L$-FDAA) 7.11 (2*S*, 3*R*, $_D$-FDAA) 5.14 (2*S*, 3*S*, $_L$-FDAA) 4.80 (2*S*, 3*S*, $_D$-FDAA)		8.30	7.10	2*S*,3*R*
γ-hyGlu	415	8.28 (2*S*, 4*R*, $_L$-FDAA) 7.03 (2*S*, 4*R*, $_D$-FDAA) 6.77 (2*S*, 4*S*, $_L$-FDAA) 7.12 (2*S*, 4*S*, $_D$-FDAA)		8.30	7.03	2*S*,4*R*

0.2 mL/min gradient elution from 80% to 40% H_2O/MeCN with 0.1% formic acid over 40 min on Thermo Acclaim 120 RP-C_{18} column, 2.1 × 150 mm, 5 μm; ESI-HRMS on the positive ion mode.

Table S4. Retention times (t_R, min) for GITC derivatives of L- or D-AMPA standards and of the hydrolysate of cadaside A (**1**)

AA	AA standards		hydrolysate of **1**
	$t_{R\ (L\text{-}AA\text{-}GITC)}$ (min)	$t_{R\ (D\text{-}AA\text{-}GITC)}$ (min)	$t_{R\ (AA\text{-}GITC)}$ (min)
L-AMPA	40.31	–	–
D-AMPA	–	38.85	38.92

1 mL/min isocratic elution at 80% H_2O/MeCN with 0.1% formic acid over 60 min on XBridge RP-C_{18} column, 2.1 × 150 mm, 5 μm, UV-vis detection at 254 nm.

Table S5. Spectrum of activity for cadasides (**1**) and B (**2**).

Strains	Gram + or –	Acquired resistance	MIC (μg/mL)		
			cadaside A	cadaside B	daptomycin
Staphylococcus aureus RN4220	+		4	4	0.25
Staphylococcus aureus USA300	+	methicillin	8	16	0.5
Staphylococcus aureus NRS100	+	oxacillin, tetracycline	1-2	2	0.25
Staphylococcus aureus NRS140	+	erythromycin, spectinomycin	1-2	2	0.25
Staphylococcus aureus NRS108	+	gentamycin, oxacillin	2	2	0.5
Staphylococcus aureus NRS146	+	vancomycin	2	2	0.25
Staphylococcus aureus ATCC 12600	+	rifampicin (*rpo*B S486L)	4	4	0.5
Bacillus subtilis ATCC 6051	+		2	2	0.125
Bacillus subtilis 168 IAI	+		4	4	0.125
Enterococcus faecium O1GRF	+		2-4	2-4	0.125
Enterococcus faecium EF16	+	vancomycin	2-4	4	0.125
Enterococcus faecium ATCC 51559	+	ampicillin ciprofloxacin gentamicin rifampin teicoplanin vancomycin	4-8	8	0.125-0.25
Staphylococcus epidermidis RP62A	+		2	2	0.5-1
Streptococcus mutans ATCC 25175	+		1	1	0.5
Streptococcus oralis ATCC 9811	+		2	2	0.0625
Escherichia coli DH5α	–		> 64	> 64	> 64
Escherichia coli BAS 849	–		32-64	> 64	> 64
Enterobacter cloacae ATCC 13047	–		> 64	> 64	> 64
Pseudomonas aeruginosa PAO1	–		> 64	> 64	> 64
Klebsiella pneumonia ATCC 10031	–		> 64	> 64	> 64
Acinetobacter baumannii ATCC 17978	–		> 64	> 64	> 64
Salmonella enterica A84	–		> 64	> 64	> 64
Proteus mirabilis ATCC 29906	–		> 64	> 64	> 64
Candida albicans ATCC 76485	yeast		> 64	> 64	> 64
Saccharomyces pombe SAK931	yeast		> 64	> 64	> 64
Saccharomyces cerevisiae W303 G1b	yeast		> 64	> 64	> 64

The antimicrobial data in the table were acquired in the presence of 100 mM of $CaCl_2$. All the values were determined on the basis of three independent experiments. 1 μg/mL = 0.64 μM for cadasides A and B.

Table S6. List of PCR primers used in this study

Primer Name	Sequence	Function
A3F [6,7]	GCSTACSYSATSTACACSTCSGG	eDNA library screening
A7R [6,7]	SASGTCVCCSGTSCGGTA	eDNA library screening
431-Fw	CGAAGGGTGTGGTGGTTGAG	Clone recovery of cosmid DFD0097-431
431-Rv	TCATGAACGAGACACCCGAC	Clone recovery of cosmid DFD0097-431
157-Fw	GTCCGAAGGGTGTGGTG	Clone recovery of cosmid DFD0097-157
157-Rv	CACCTGATCCCTCGTCG	Clone recovery of cosmid DFD0097-157
262-Fw	TCAGGAGGACCATGTCCGAG	Clone recovery of cosmid DFD0097-262
262-Rv	CTCAGACCAGCGGTGTGTAG	Clone recovery of cosmid DFD0097-262
cde-157-UPS_Fw	GCCCCGTTAACCCCGGCTTCGACCTGTCCGTCGAAC	Upstream homology arm for TAR
cde-157-UPS_Rv	ATCTTGCCGTTGGTTTAAACGTACGTCAGGGAGCGGTCACC	Upstream homology arm for TAR
cde-262-DWS_Fw2	GTTTAAACCAACGGCAAGATCTACCGCGG	Downstream homology arm for TAR
cde-262-DWS_Rv2	CCCTGCAGGAGCTCGCGTTGTCGAACGAGGTGTAGG	Downstream homology arm for TAR
TAR_check1_Fw	CTCATCGACACGTGGCTCAAG	Check TAR fidelity by primer-walking PCR
TAR_check1_Rv	TCCAGGGAGAAGACGATCTGC	Check TAR fidelity by primer-walking PCR
TAR_check2_Fw	GCACACTTCTACATCCGCGAG	Check TAR fidelity by primer-walking PCR
TAR_check2_Rv	GAGATCGTAGGTGTACGAGCC	Check TAR fidelity by primer-walking PCR
TAR_check3_Fw	GTCCGAAGGGTGTGGTG	Check TAR fidelity by primer-walking PCR
TAR_check3_Rv	CACCTGATCCCTCGTCG	Check TAR fidelity by primer-walking PCR
TAR_check4_Fw	GACTGCTCCGCTACCTCAAC	Check TAR fidelity by primer-walking PCR
TAR_check4_Rv	CAGGTGTGAGAGGTCGGCTT	Check TAR fidelity by primer-walking PCR
TAR_check5_Fw	GATGACCAGGTGAAGGTGC	Check TAR fidelity by primer-walking PCR
TAR_check5_Rv	GTGATGTTCTCCGTGCTCG	Check TAR fidelity by primer-walking PCR
TAR_check6_Fw	GATACCGTGGACAACCACGC	Check TAR fidelity by primer-walking PCR
TAR_check6_Rv	GCGAGATCACCGCGTATCTC	Check TAR fidelity by primer-walking PCR

Figure S1. Phylogenetic tree of AD NPSTs identified by eSNaPD analysis. The tree contains 33 metagenomic library Asp4 related NPSTs (e-value < 10^{-40}) and trimmed Asp4 AD domain sequences from reference calcium-dependent antibiotic gene clusters. 18 cosmid clones associated with Asp4 NPSTs were recovered from the eDNA libraries and PGM sequenced. The amino acid specificity of each AD domain found on these clones was bioinformatically predicted and annotated on the tree in blue color. The cosmid DFD0097-431 encoding cadaside is highlighted in yellow.

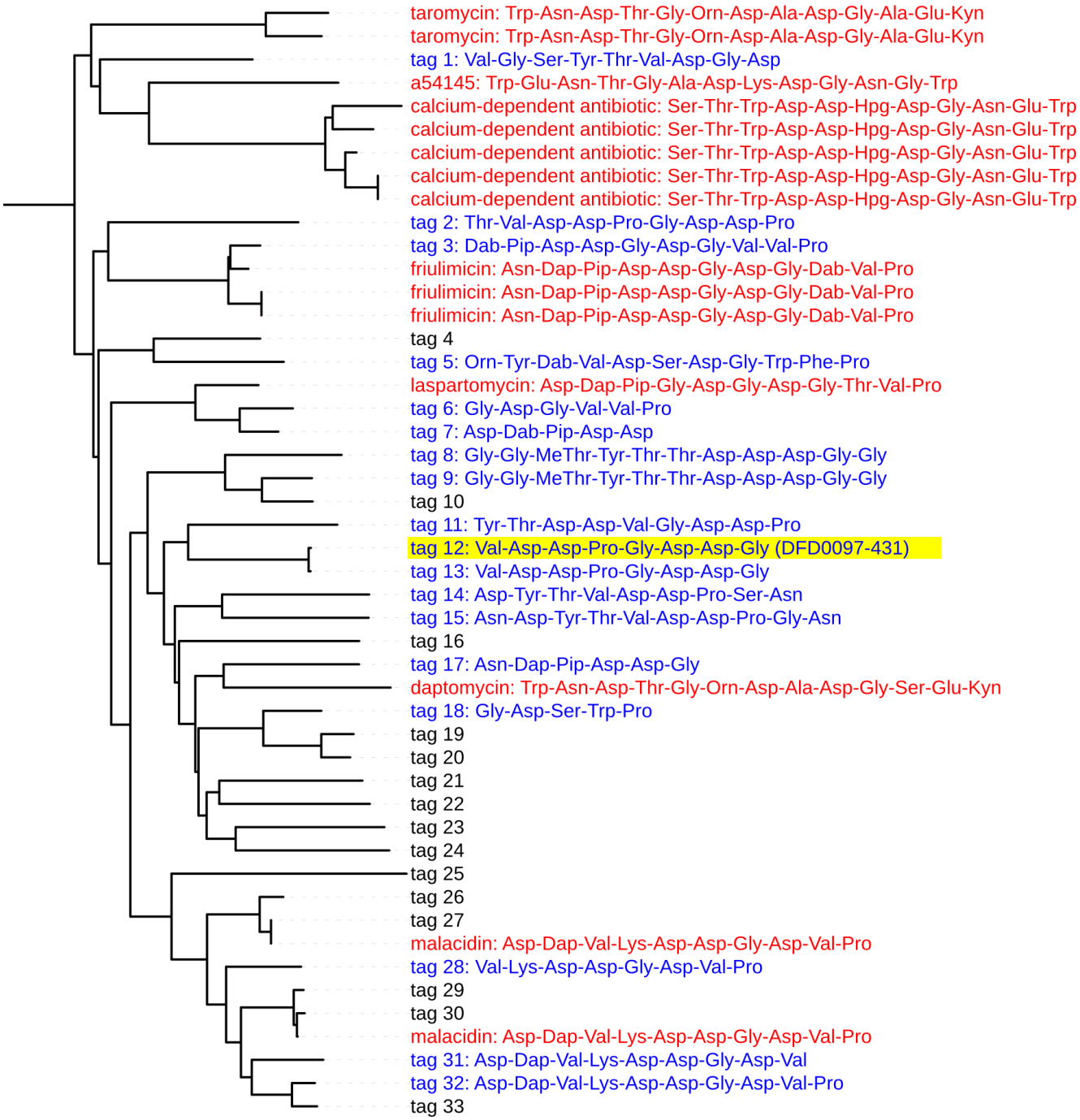

Figure S2. Comparison of the biosynthetic gene clusters for cadasides and other calcium-dependent antibiotics. NRPS genes are indicated in light blue with domain architecture and incorporated amino acids listed below each gene. The rest of the genes are colored by predicted functions: regulator (green), transporter (yellow), amino acid biosynthesis (purple), and fatty acid biosynthesis (red). Table of relationships between *cde* genes and their closest relatives found in other calcium-dependent antibiotic gene clusters. Percent identity is shown in parenthesis. The genes exclusive to *cde* gene cluster are those predicted to be responsible for the biosynthesis of nonproteinogenic amino acids AMPA and D-Ile.

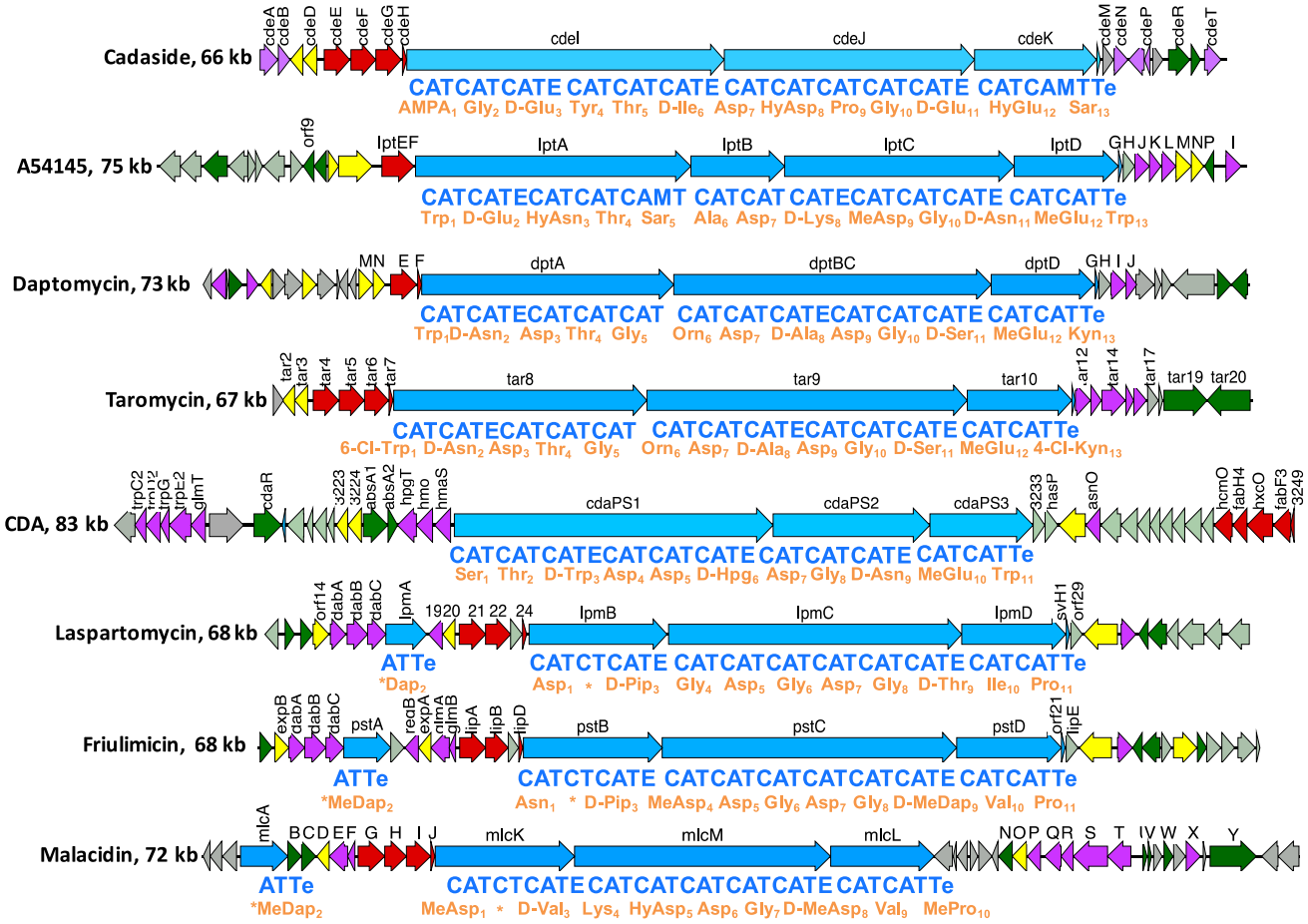

Cadaside	Malacidin (eDNA)	Laspartomycin (*Streptomyces viridochromogenes*)	Friulimicin (*Actinoplanes friuliensis*)	A54145 (*Streptomyces. fradiae*)	CDA (*Streptomyces coelicolor*)	Daptomycin (*Streptomyces roseosporus*)	Taromycin (*Saccharomonospora sp. CNQ490*)
CdeA	–	–	–	–	–	–	–
CdeB	–	Orf29 (67%)	LipE (63%)	LptH (57%)	SCO3233 (62%)	DapH (60%)	Tar17 (32%)
CdeC	MlcD (52%)	Orf20 (46%)	ExpA (53%)	LptN (49%)	SCO3223 (35%)	DapN (52%)	Tar2 (47%)
CdeD	MlcO (62%)	Orf14 (60%)	ExpB (61%)	LptM (57%)	SCO3224 (33%)	DapM (62%)	Tar3 (62%)
CdeE	MlcG (54%)	Orf21 (50%)	LipA (52%)	LptEF (45%)	–	DapE (48%)	Tar4 (45%)
CdeF	MlcH (58%)	Orf22 (50%)	LipB (50%)	–	–	–	Tar5 (51%)
CdeG	MlcI (55%)	–	–	–	–	–	Tar6 (50%)
CdeH	MlcJ (47%)	Orf24 (64%)	LipD (58%)	–	–	DapF (42%)	Tar6 (36%)
CdeI	MlcM (44%)	LpmC (50%)	PstC (51%)	LptC (47%)	CdaPS1 (47%)	DapBC (45%)	Tar9 (45%)
CdeJ	MlcL (56%)	LpmC (54%)	PstC (53%)	LptC (48%)	CdaPS1 (49%)	DapBC (48%)	Tar8 (50%)
CdeK	MlcM (48%)	LpmD (51%)	PstD (50%)	LptD (52%)	CdaPS3 (52%)	DapD (52%)	Tar10 (51%)
CdeL	MlcV (76%)	SvH1 (72%)	Orf21 (75%)	LptG (65%)	CdaPS2 (72%)	DapG (66%)	Tar11 (72%)
CdeM	–	–	–	–	–	–	–
CdeN	MlcC (69%)	Orf19 (32%)	RegB (34%)	LptJ (60%)	AsnO (35%)	–	–
CdeO	–	–	–	–	–	–	–
CdeP	–	–	–	–	–	–	–
CdeQ	–	–	–	–	–	–	–
CdeR	–	–	–	–	AbsA1 (45%)	–	–
CdeS	–	–	–	Orf9 (48%)	AbsA2 (60%)	–	–
CdeT	–	–	–	–	–	–	–

Figure S3. High-resolution mass spectra of cadasides A (**1**) and B (**2**)

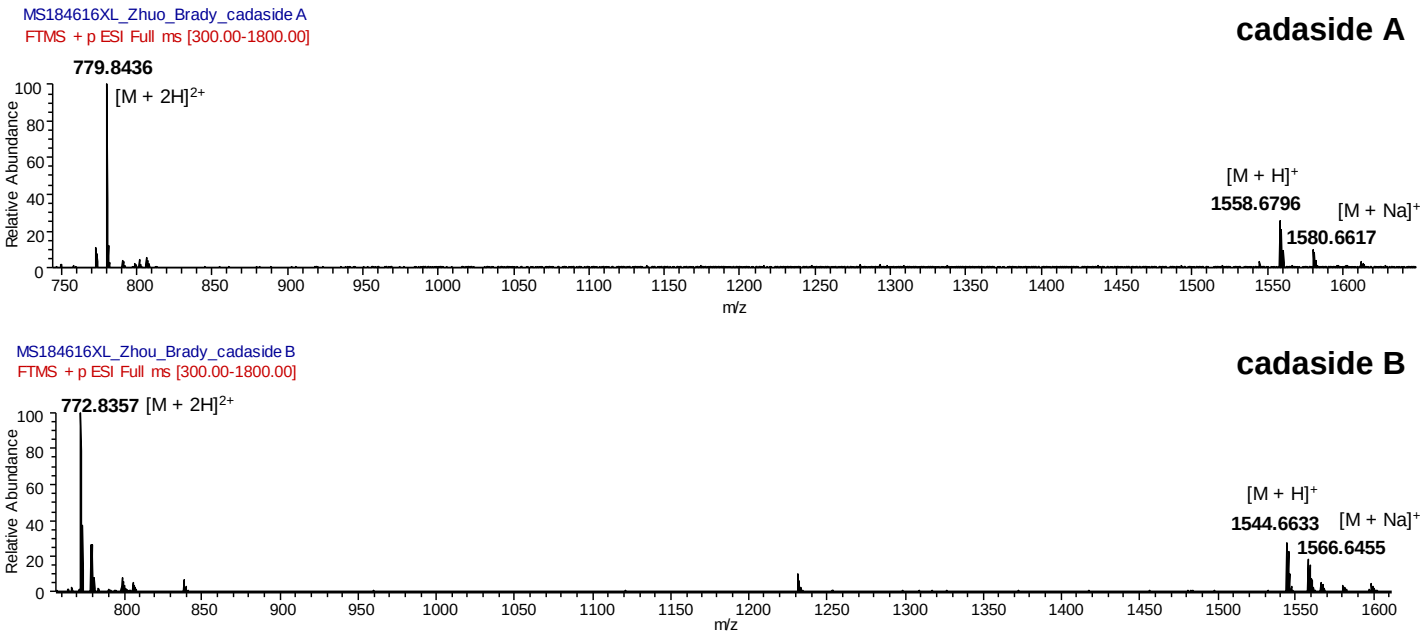

Figure S4. Structure characterization of cadaside A using 2D NMR correlations. **A**) The structure of each amino acid residue and the fatty acid side chain were assigned using COSY, TOCSY and HMBC correlations. **B**) The key 2D NMR correlations observed between α protons of amino acid residues and carbonyl carbons are shown. Based on this data, five partial structures were determined.

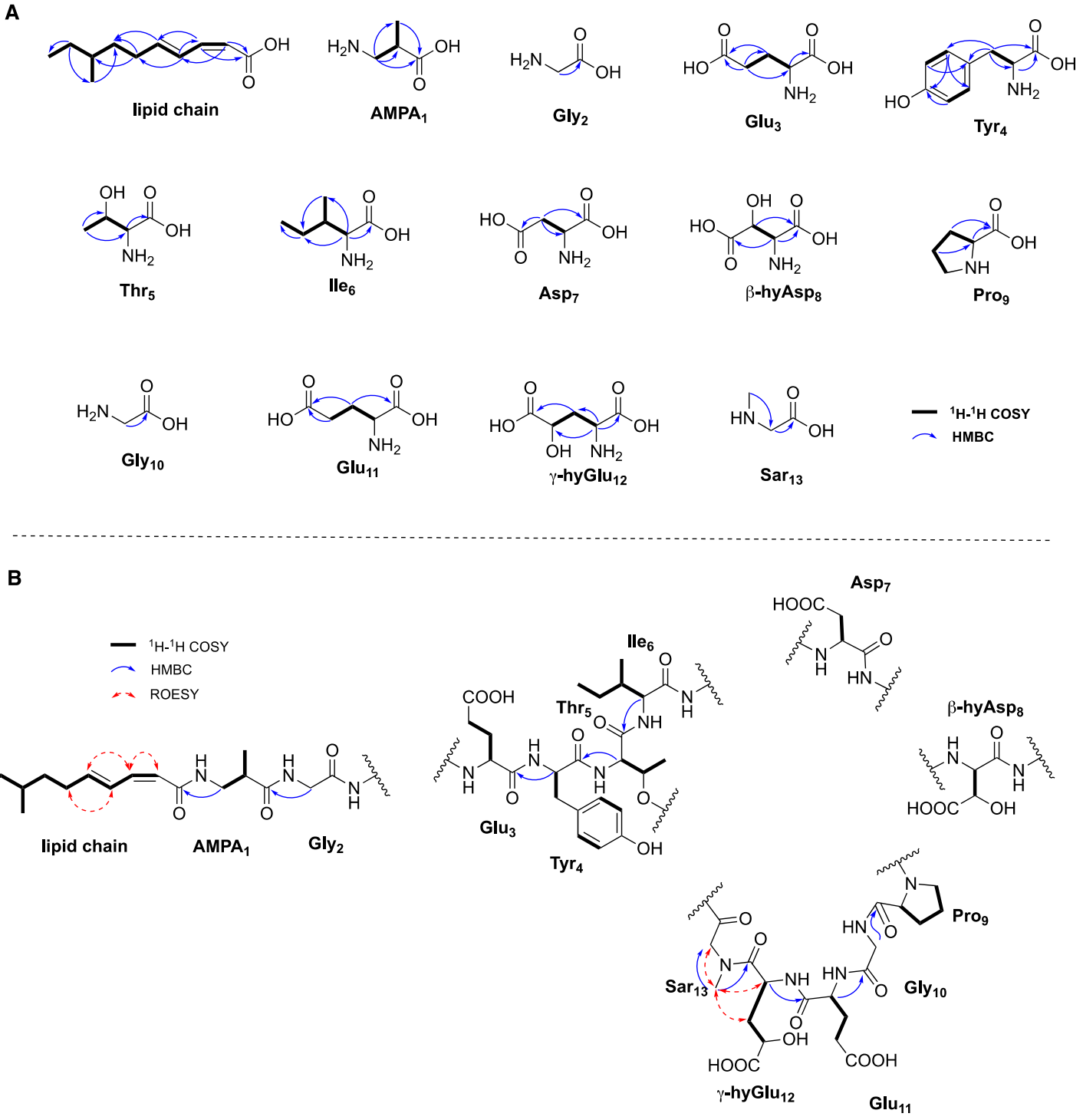

Figure S5. ESI-CID-MS/MS fragmentation of cadasides A (**1**) and B (**2**)

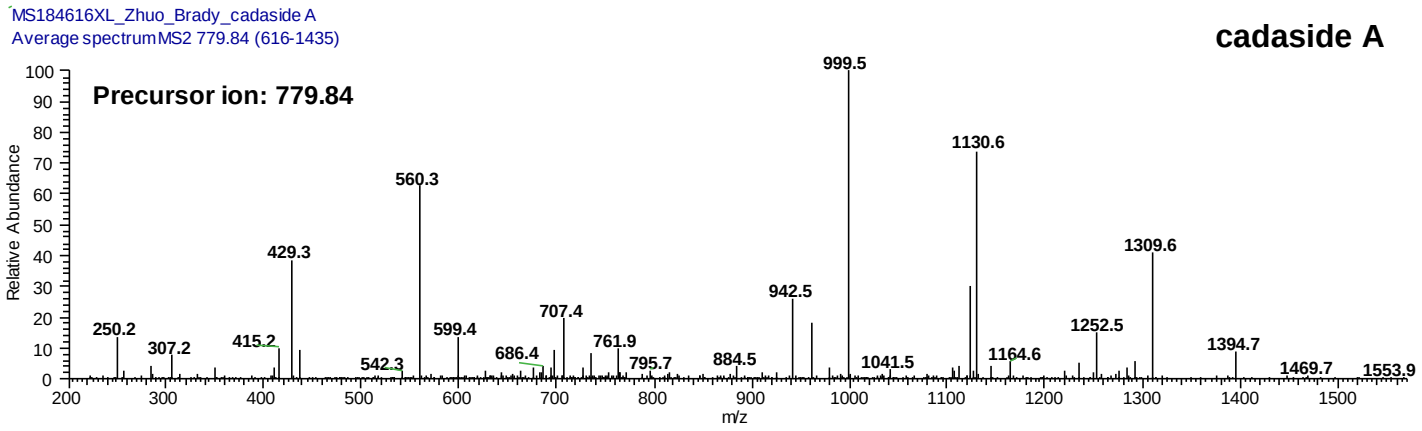

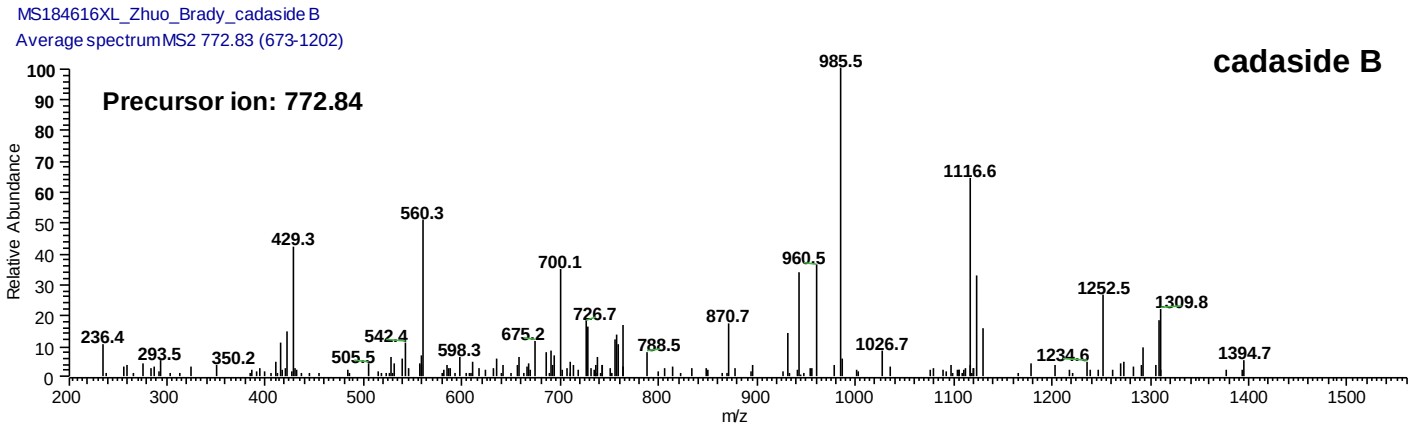

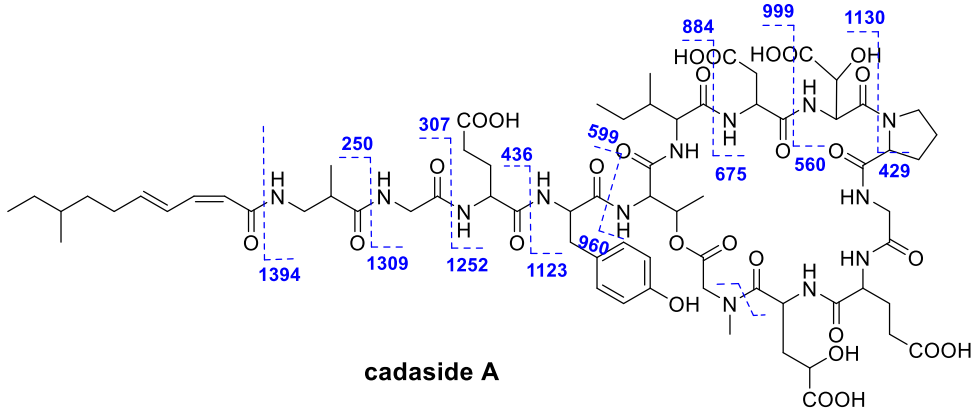

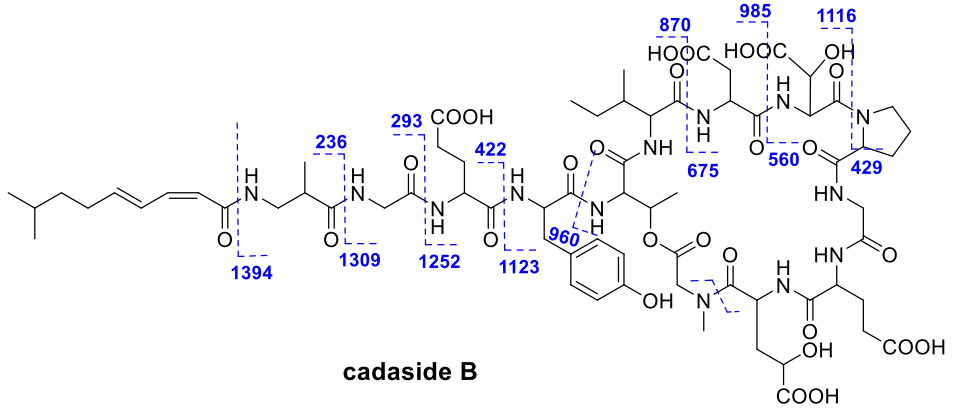

Figure S6. Annotated ESI-CID-MS/MS fragments of cadaside A (**1**)

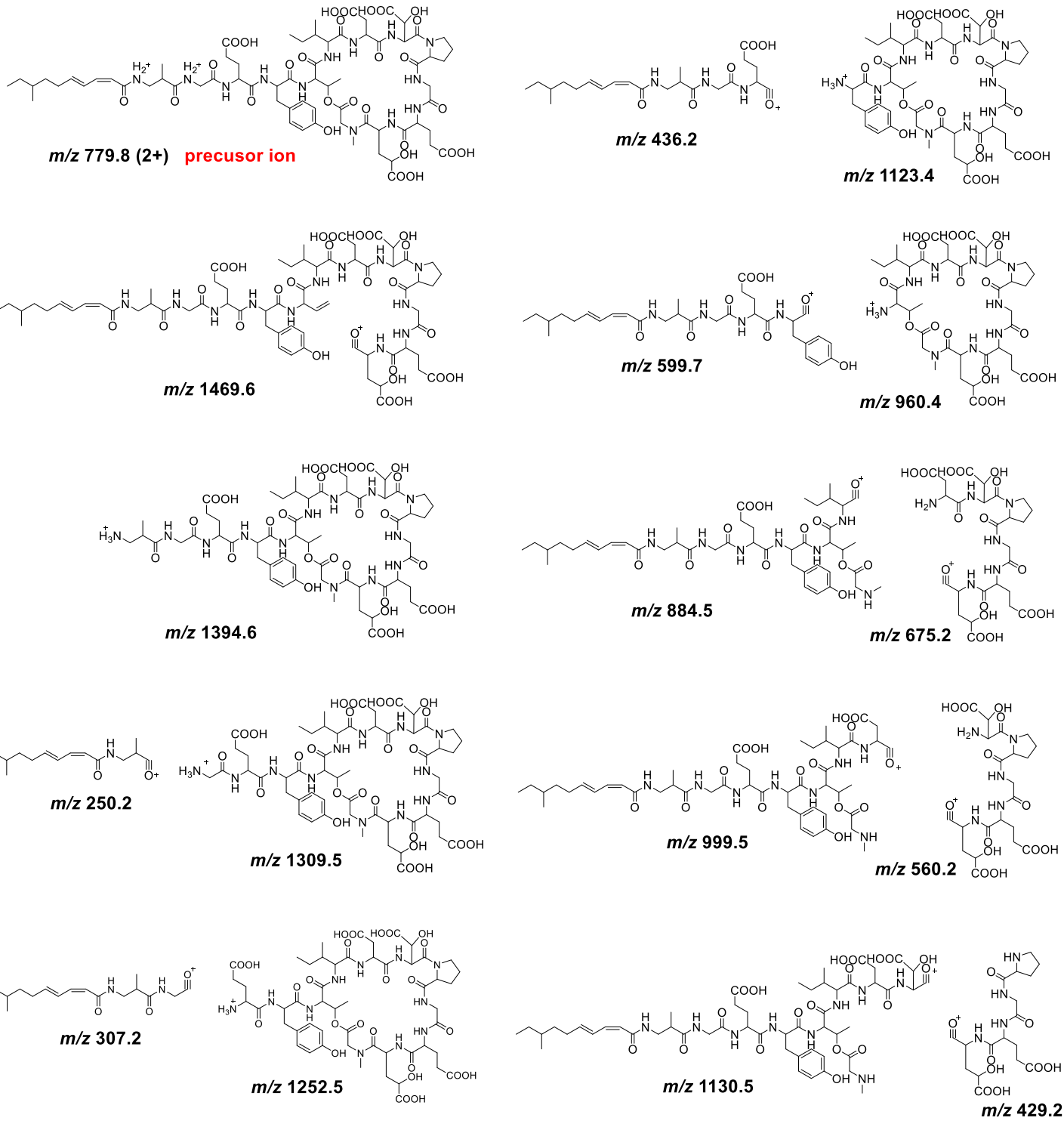

Figure S7. Key 2D NMR correlations for cadaside B (**2**)

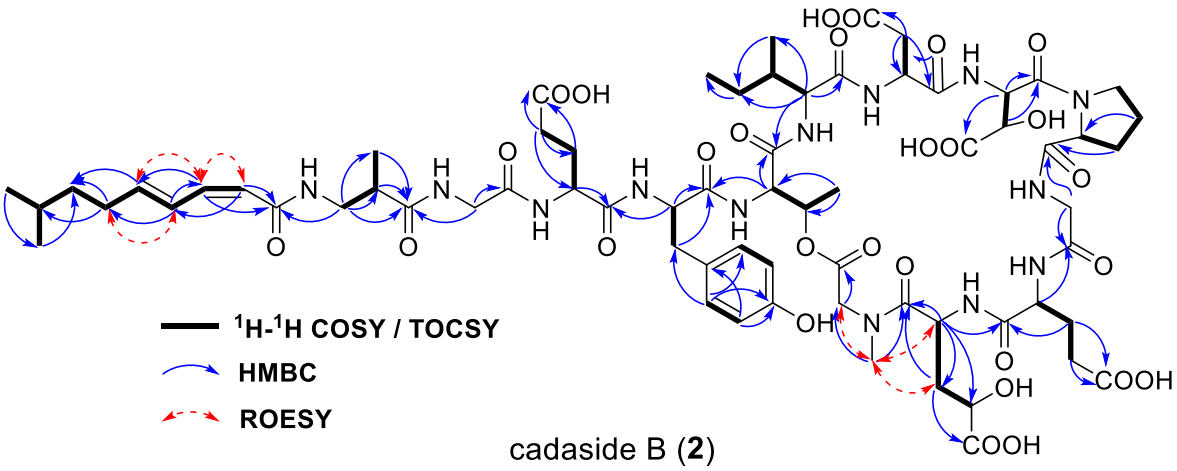

cadaside B (**2**)

Figure S8. Extracted ion chromatogram of L- and D-FDAA derivatives of the hydrolysate of cadaside A (**1**)

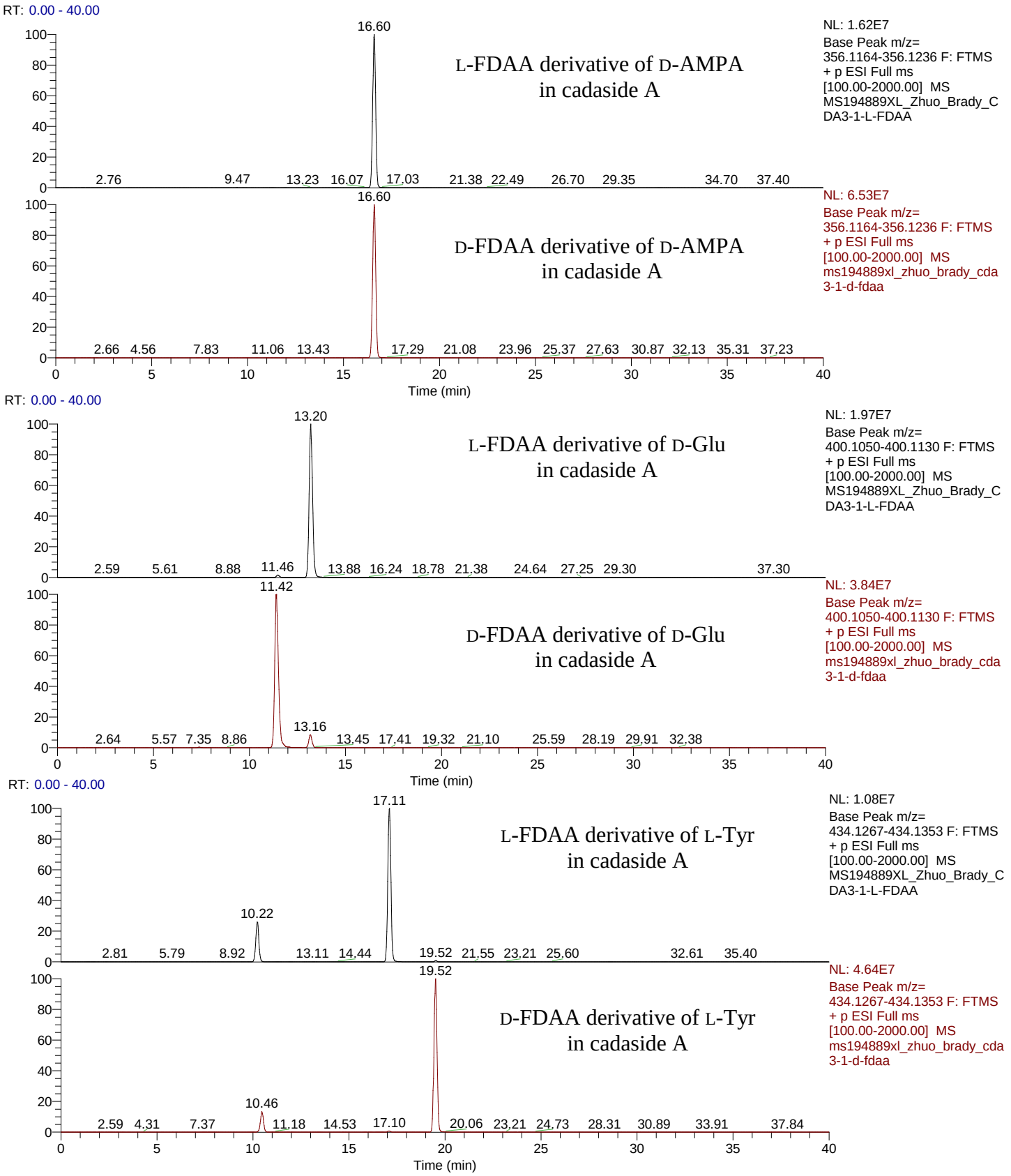

Figure S8 (continued). Extracted ion chromatogram of L- and D-FDAA derivatives of the hydrolysate of cadaside A (**1**)

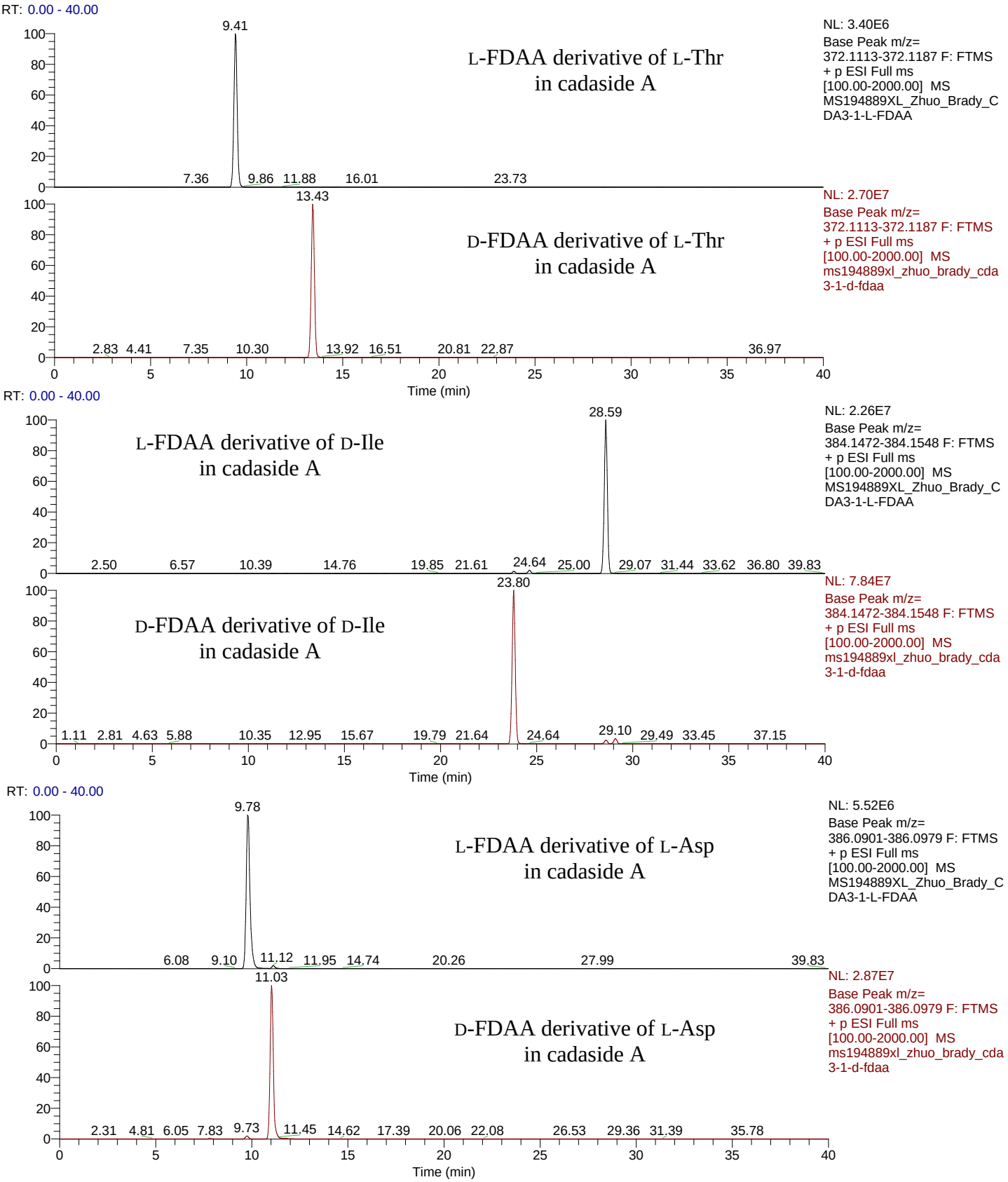

Figure S8 (continued). Extracted ion chromatogram of L- and D-FDAA derivatives of the hydrolysate of cadaside A (**1**)

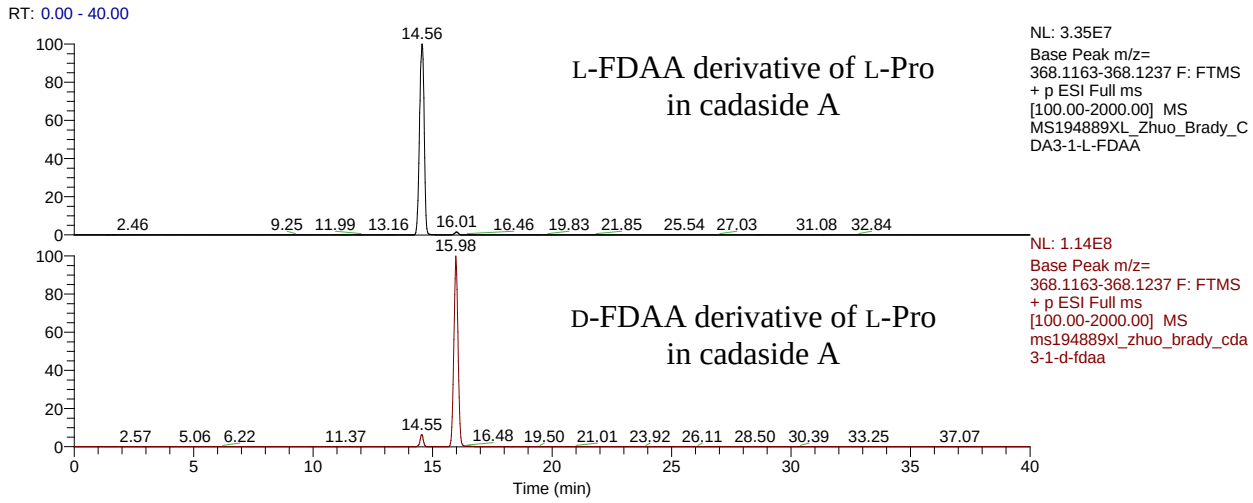

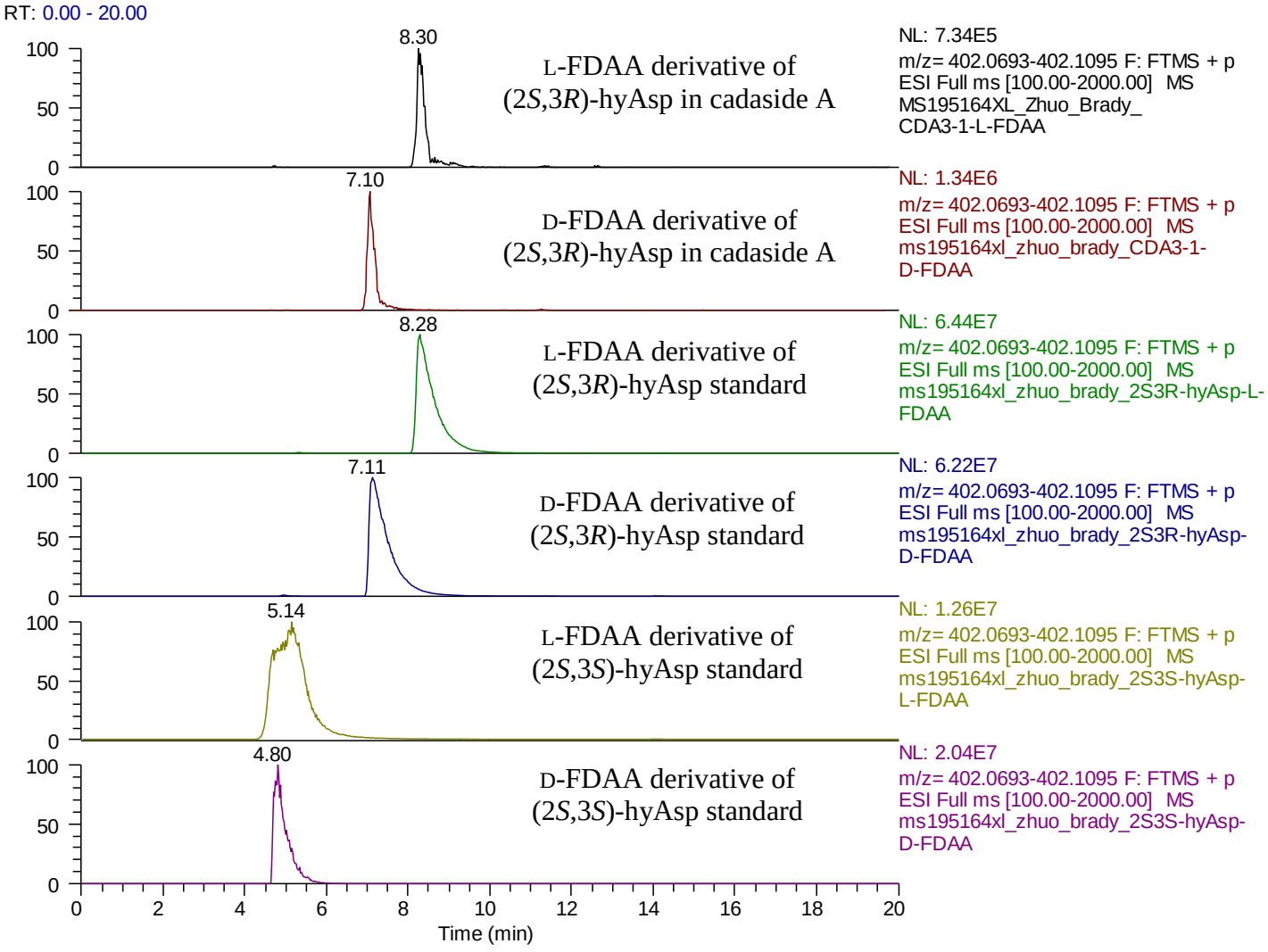

Figure S8 (continued). Extracted ion chromatogram of L- and D-FDAA derivatives of the hydrolysate of cadaside A (**1**)

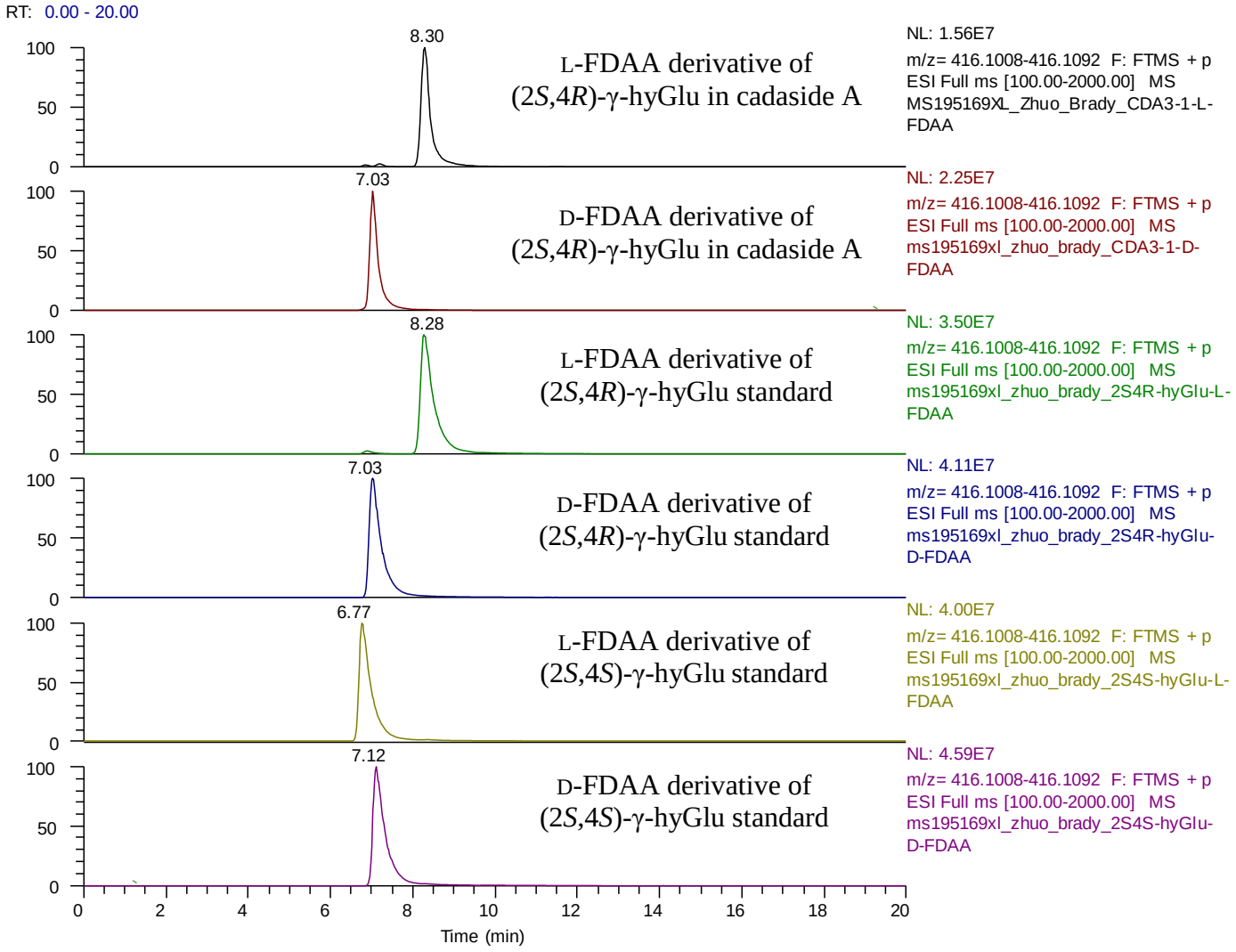

Figure S9. HPLC-DAD analysis of GITC derivatives of cadaside A hydrolysate and L/D-AMPA standards indicated that the presence of D-AMPA in cadaside A.

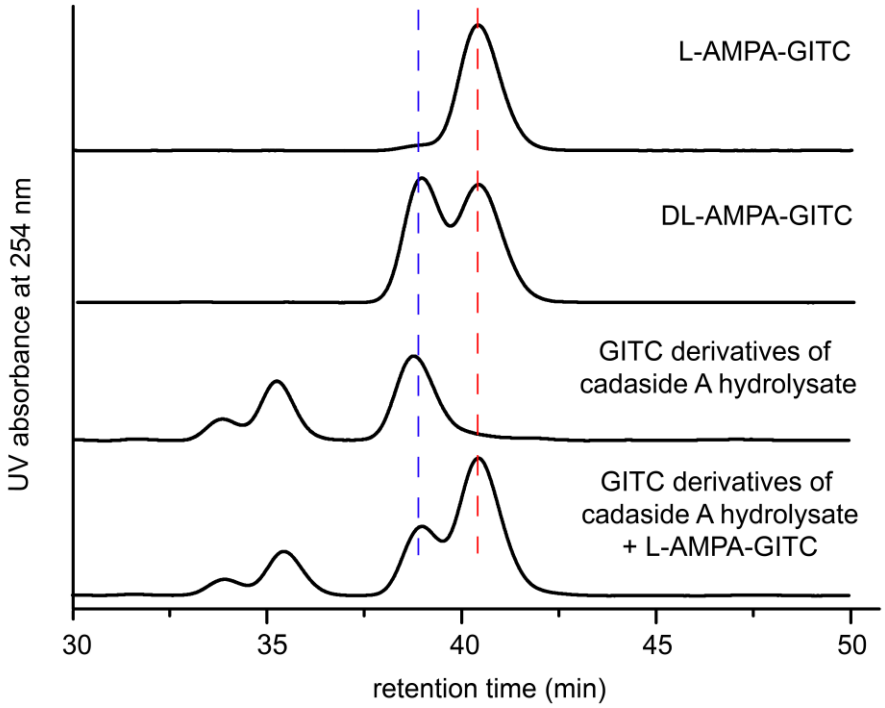

Figure S10. Proposed biosynthetic pathway for cadaside A. Cadaside A biosynthesis is predicted to follow an orthodox colinear extension model of modular NRPS system. The putative functions of key biosynthetic enzymes encoded by the *cde* gene cluster are highlighted. ACP, acyl carrier protein; C, condensation domain; A, adenylation domain; TE, thioesterase domain; T, thiolation domain; E, epimerization domain; nMT, *N*-methyltransferase domain. The proposed biosynthetic pathways of the nonproteinogenic amino acids β-hyAsp, γ-hyGlu,[8,9] D-Ile,[10] and AMPA,[11–13] are shown in the box.

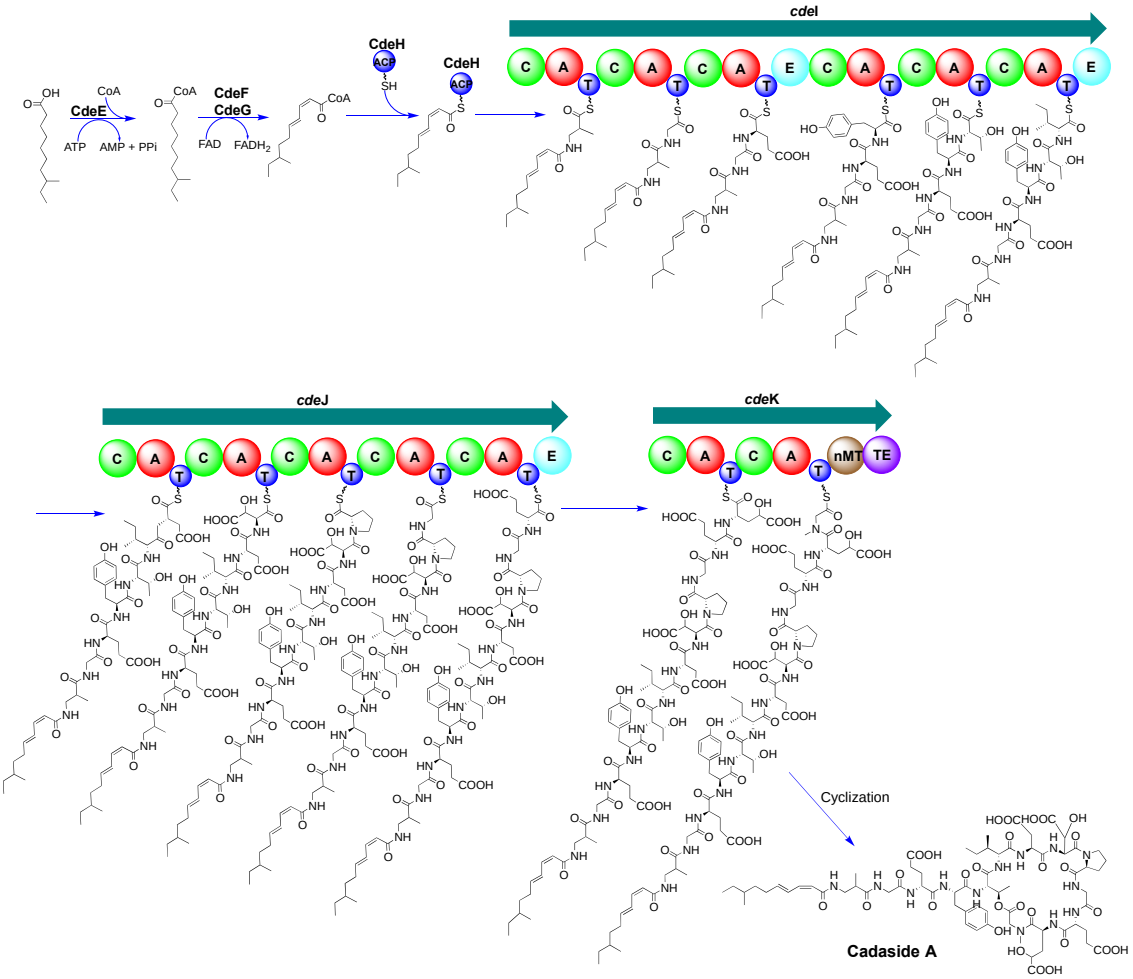

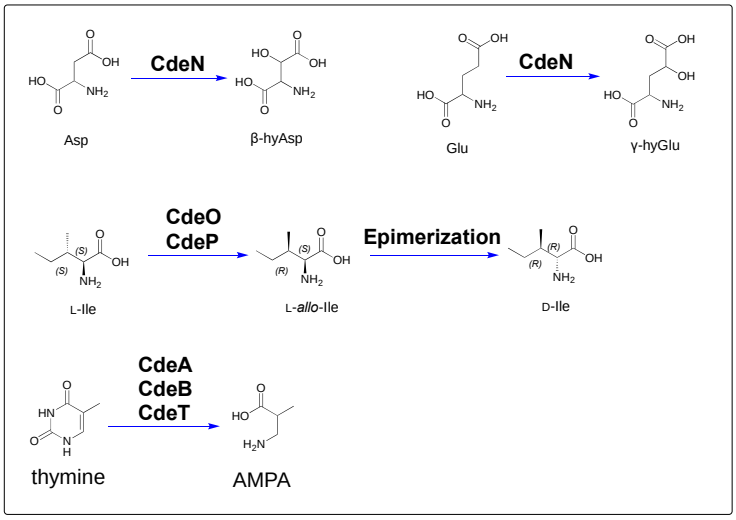

Figure S11. ^{13}C labelling confirms that the AMPA residue in cadaside A originates from thymine. (**A**) HRMS comparison of cadaside A (**1**) produced by $^{13}CH_3$-thymine fed cultures with that produced by control cultures supplemented with unlabeled thymine. When normalized to the ^{12}C peak (*m/z* 779.8422), the peak containing a single ^{13}C atom (*m/z* 780.3437) is enriched by ~30% in the $^{13}CH_3$-thymine fed cultures. The red asterisk marks peak containing a single ^{13}C atom; (**B**) CID-FT MS/MS analysis of the parental ion at *m/z* 780.34 from both ^{13}C fed and unlabeled cultures. The red and blue peaks for each fragment ion correspond to molecules containing a single ^{13}C atom and those containing only ^{12}C, respectively. The ratio of the ^{13}C containing peak to the uniform ^{12}C peak (^{13}C/^{12}C) for each fragment ion revealed that enrichment of the ^{13}C labeled peak for only those fragments (left column) containing an AMPA residue.

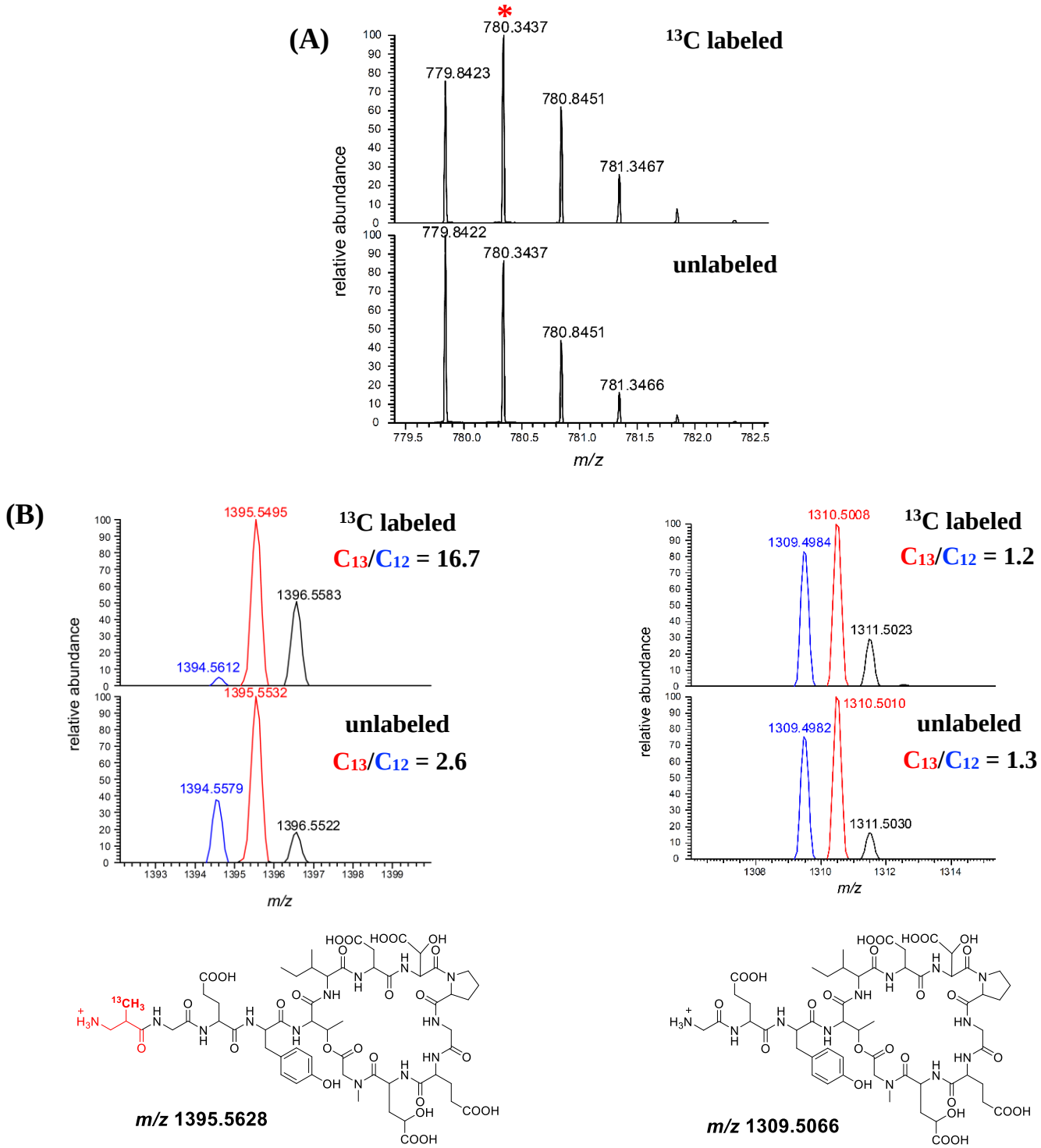

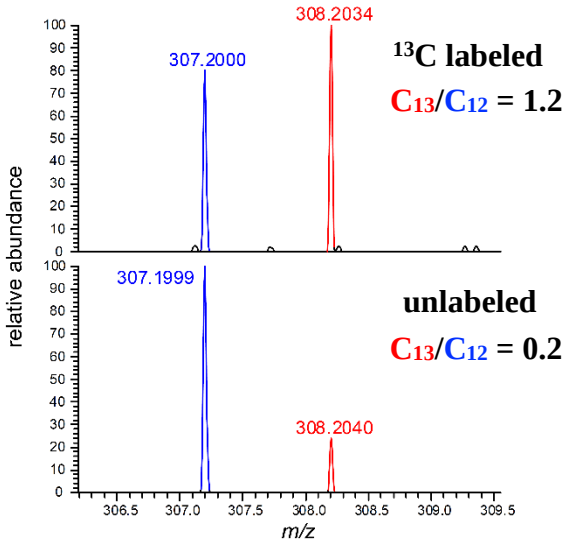

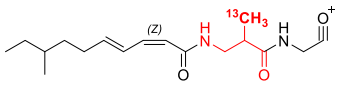

***m/z* 308.2050**

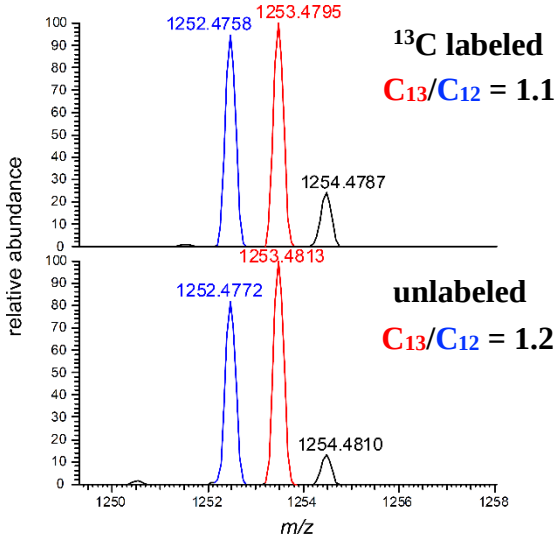

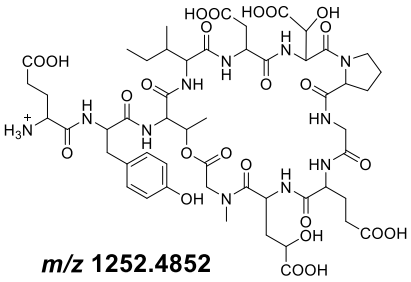

***m/z* 1252.4852**

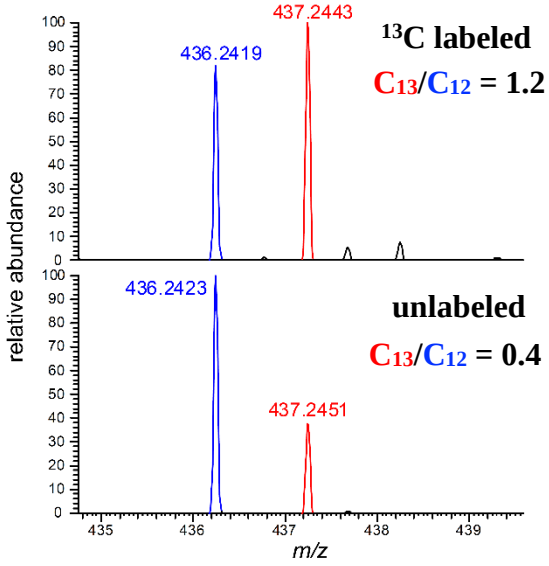

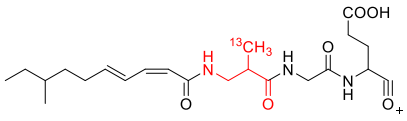

***m/z* 437.2476**

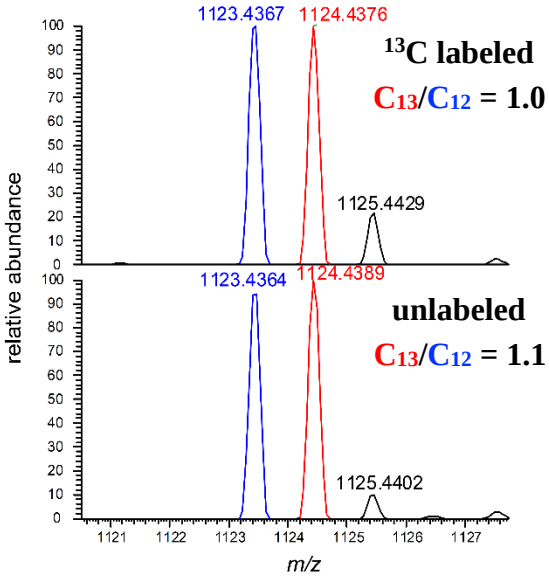

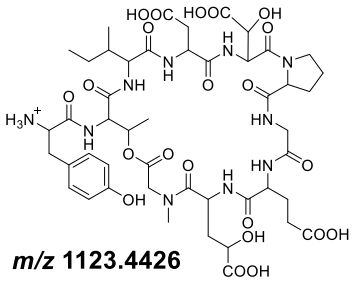

***m/z* 1123.4426**

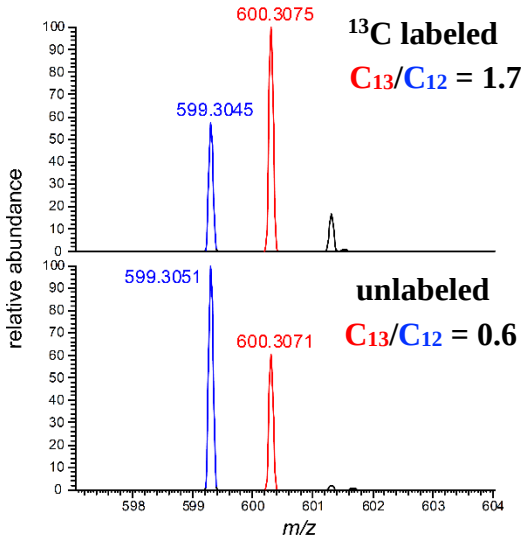

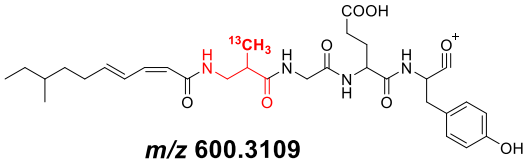

m/z 600.3109

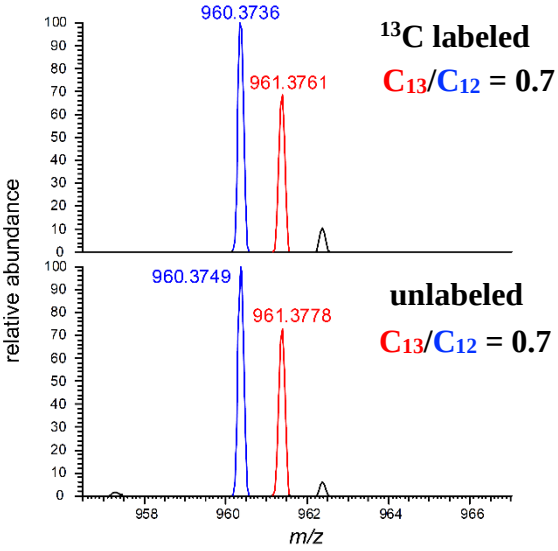

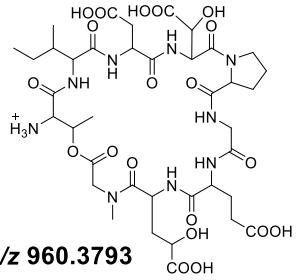

m/z 960.3793

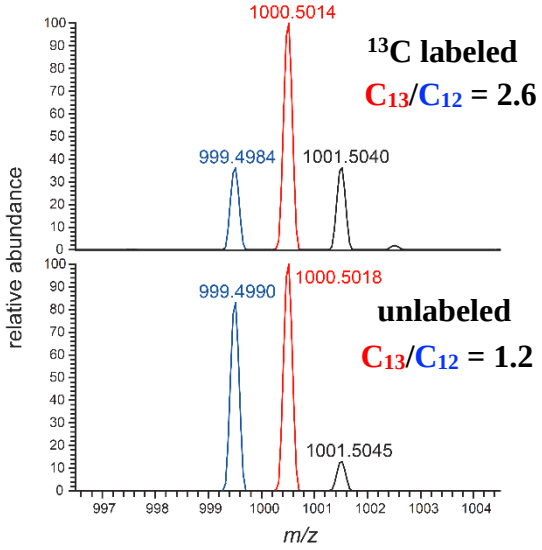

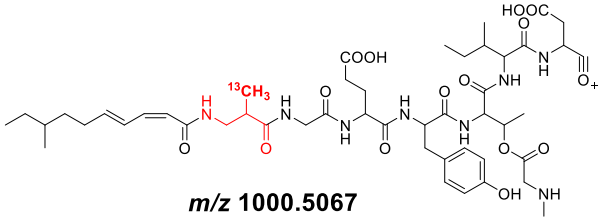

m/z 1000.5067

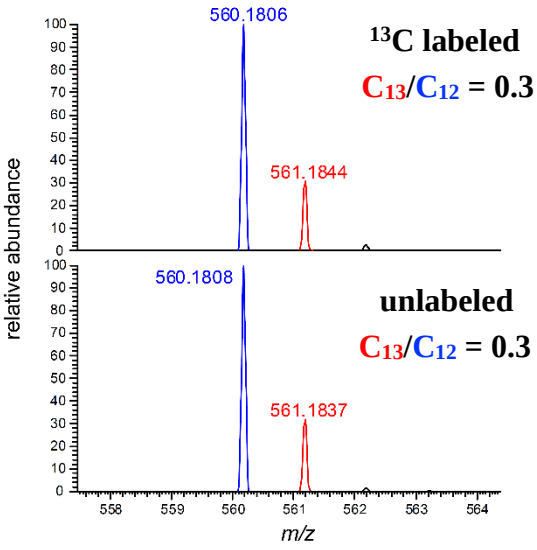

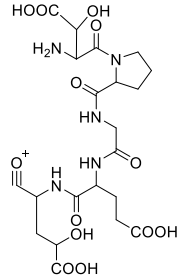

m/z 560.1835

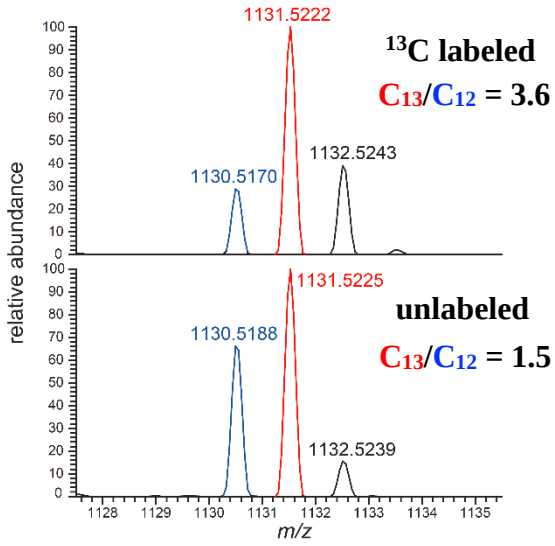

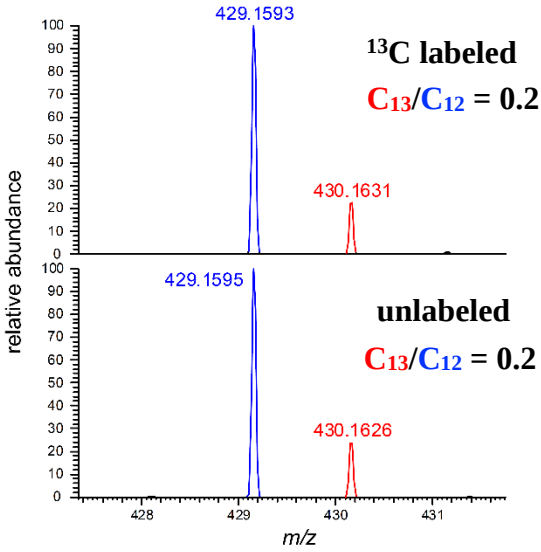

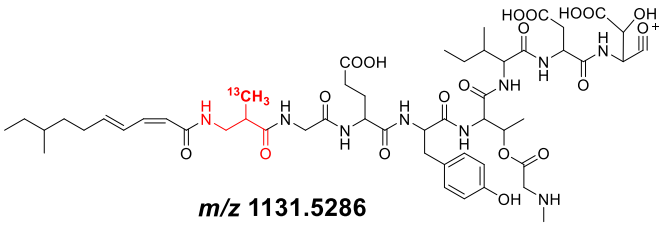

***m/z* 1131.5286**

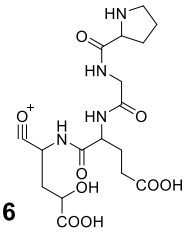

***m/z* 429.1616**

Figure S12. Cadaside A does not depolarize the bacterial cell membrane in a $DiBAC_4$ fluorescence assay. *S.aureus* NRS100 membrane depolarization ability of cadaside A (**1**), daptomycin (positive control) and vancomycin (negative control) with and without the addition of 100 mM $CaCl_2$. The error bars represent the standard deviation of three replicates.

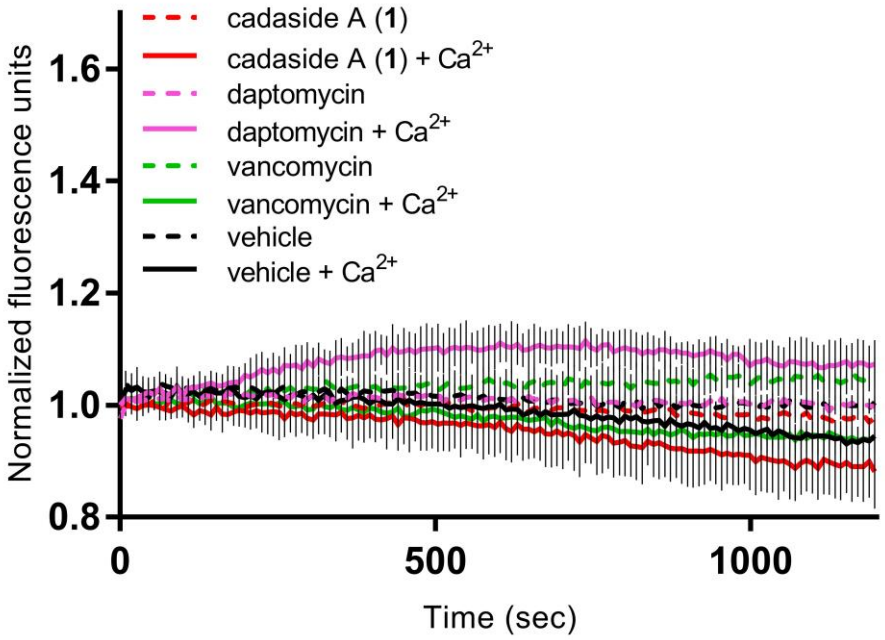

Figure S13. Chrome azurol S (CAS) assay for cadaside A, daptomycin and other siderophores.

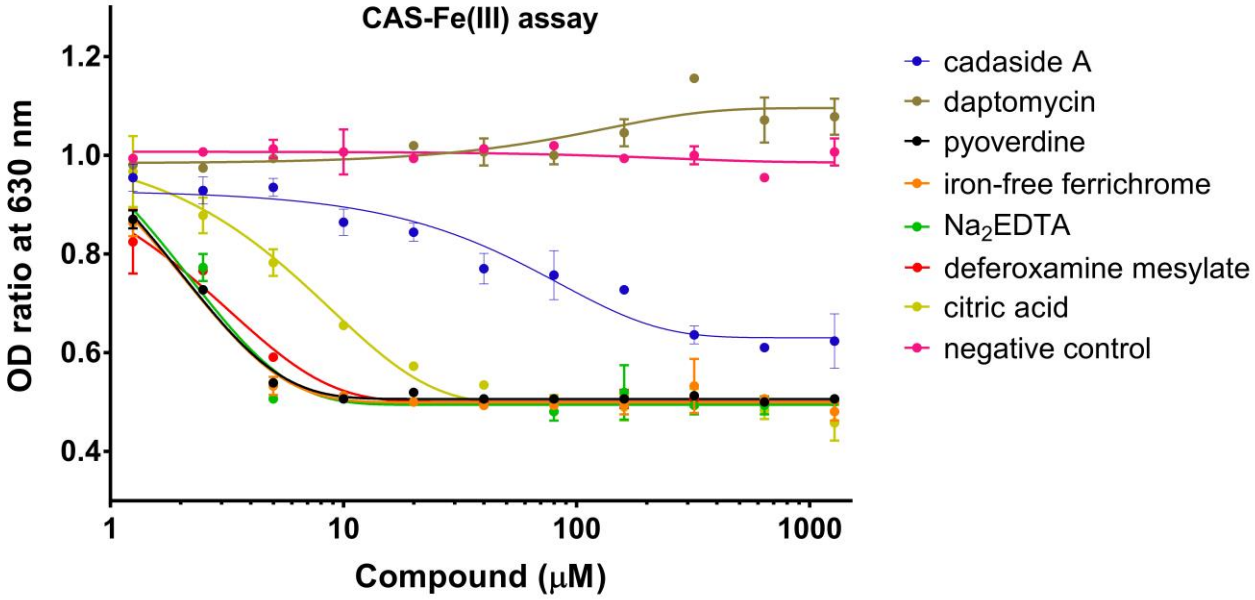

Figure S14. ^{1}H NMR (600 MHz, CD_3OD) and UV-vis spectra of cadaside A (**1**)

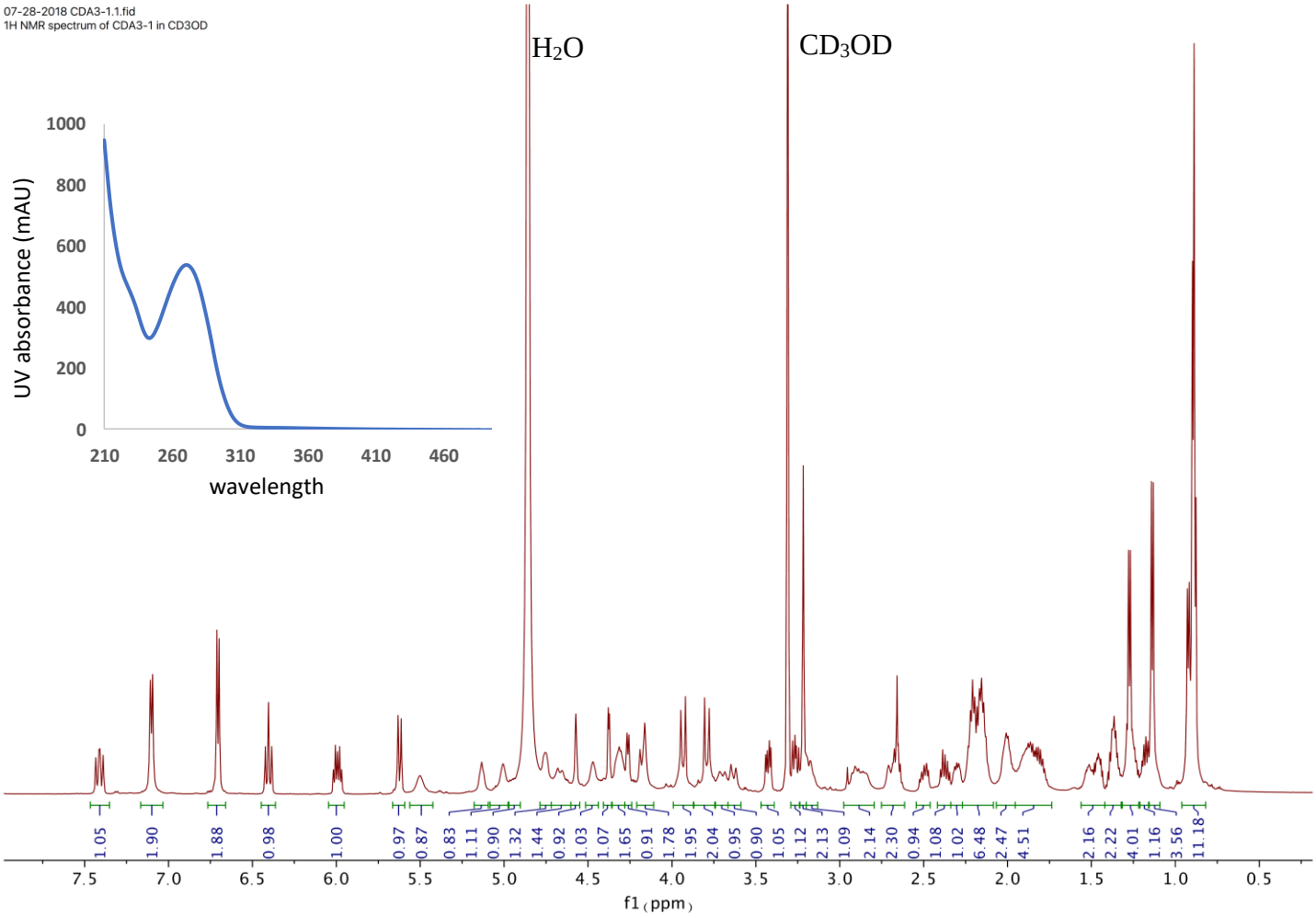

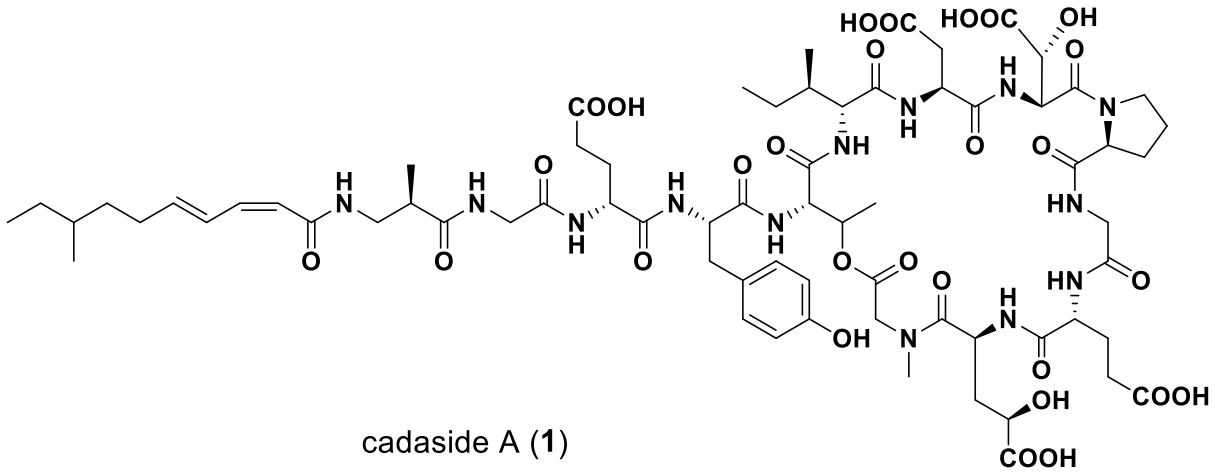

cadaside A (**1**)

Figure S15. ^{13}C NMR (150 MHz, CD_3OD) spectrum of cadaside A (**1**)

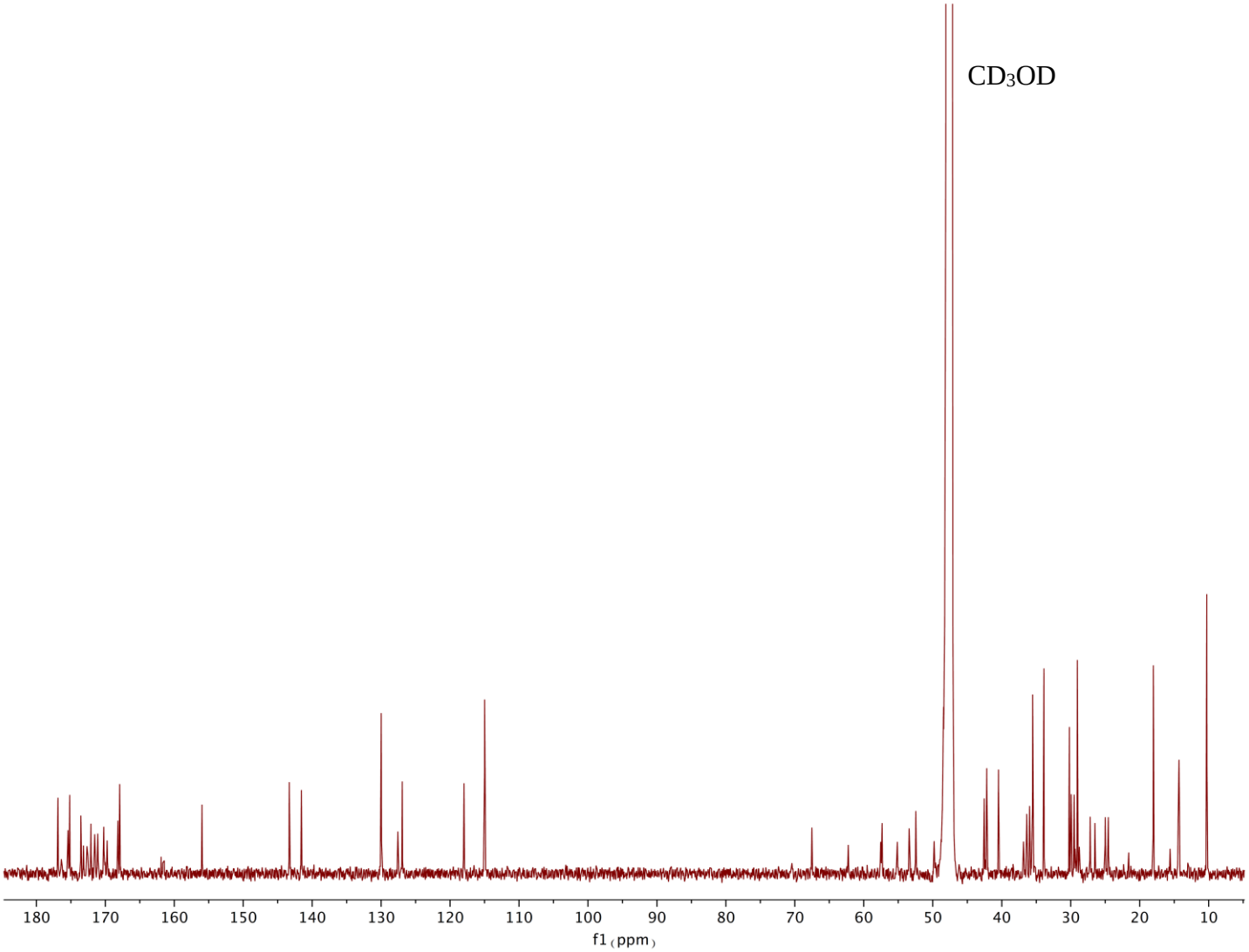

Figure S16. ^{1}H-^{13}C HSQC NMR (600 MHz, CD_3OD) spectrum of cadaside A (**1**)

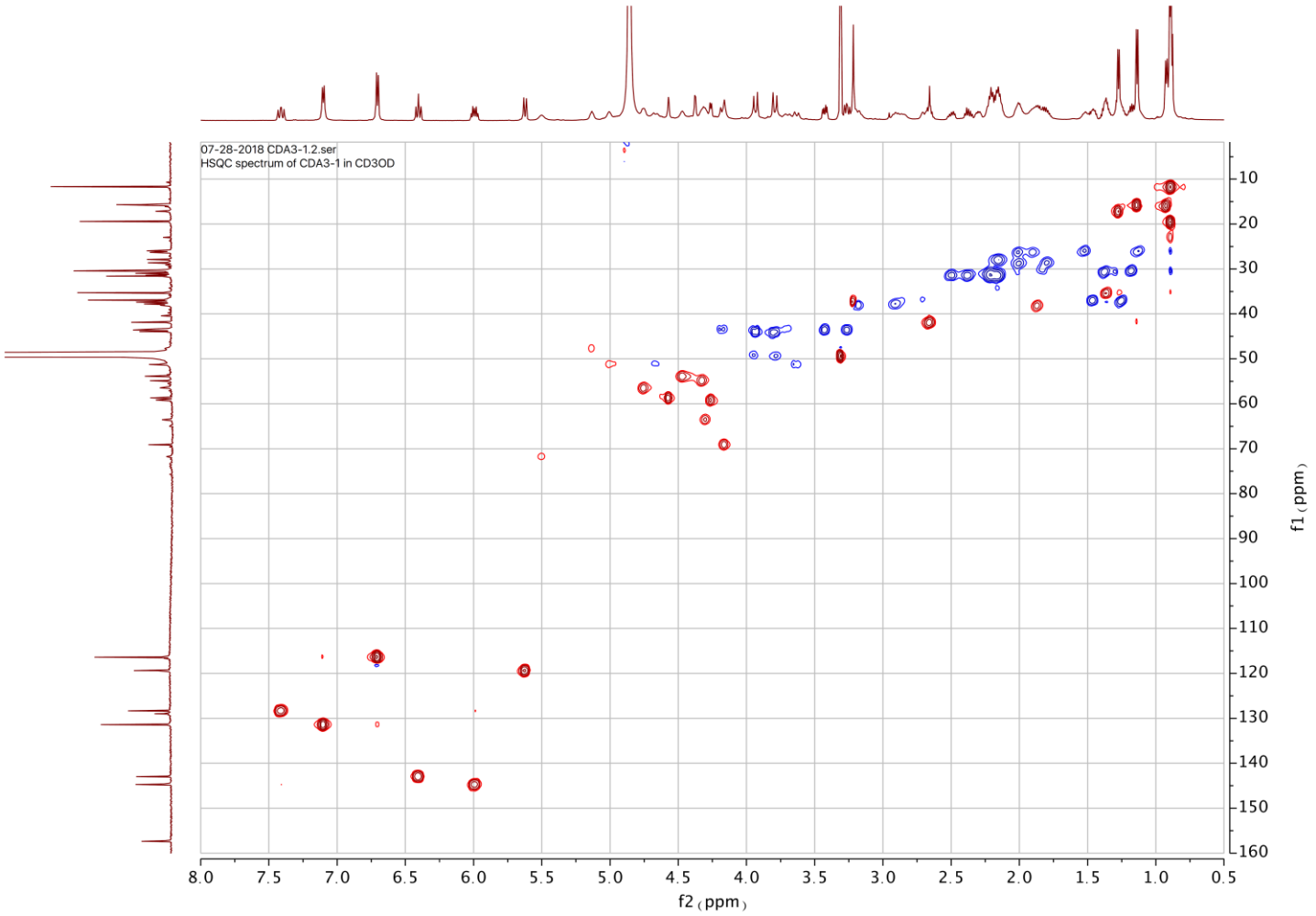

Figure S17. ^{1}H-^{13}C HMBC NMR (600 MHz, CD_3OD) spectrum of cadaside A (**1**)

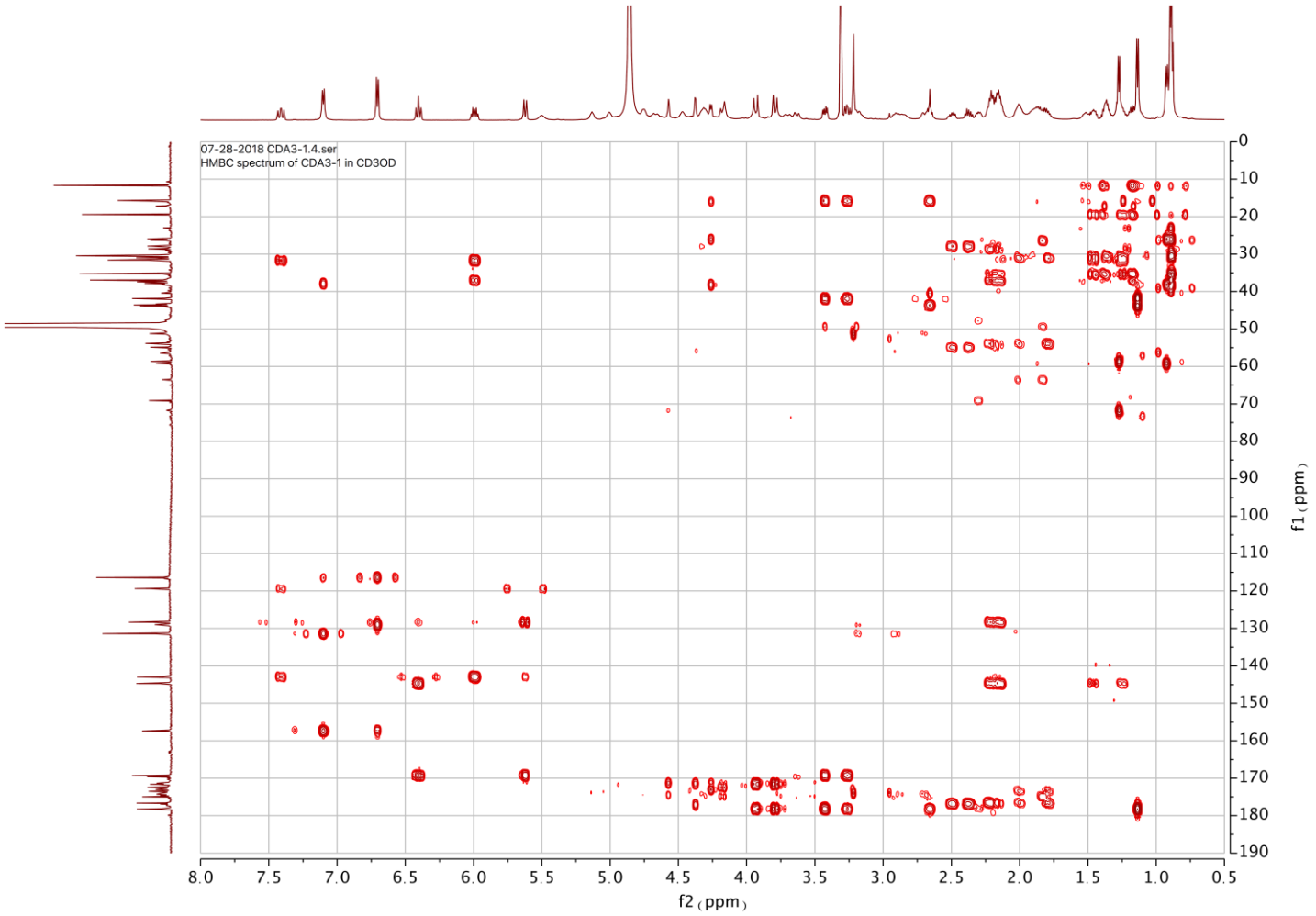

Figure S18. ^{1}H-^{1}H COSY NMR (600 MHz, CD_3OD) spectrum of cadaside A (**1**)

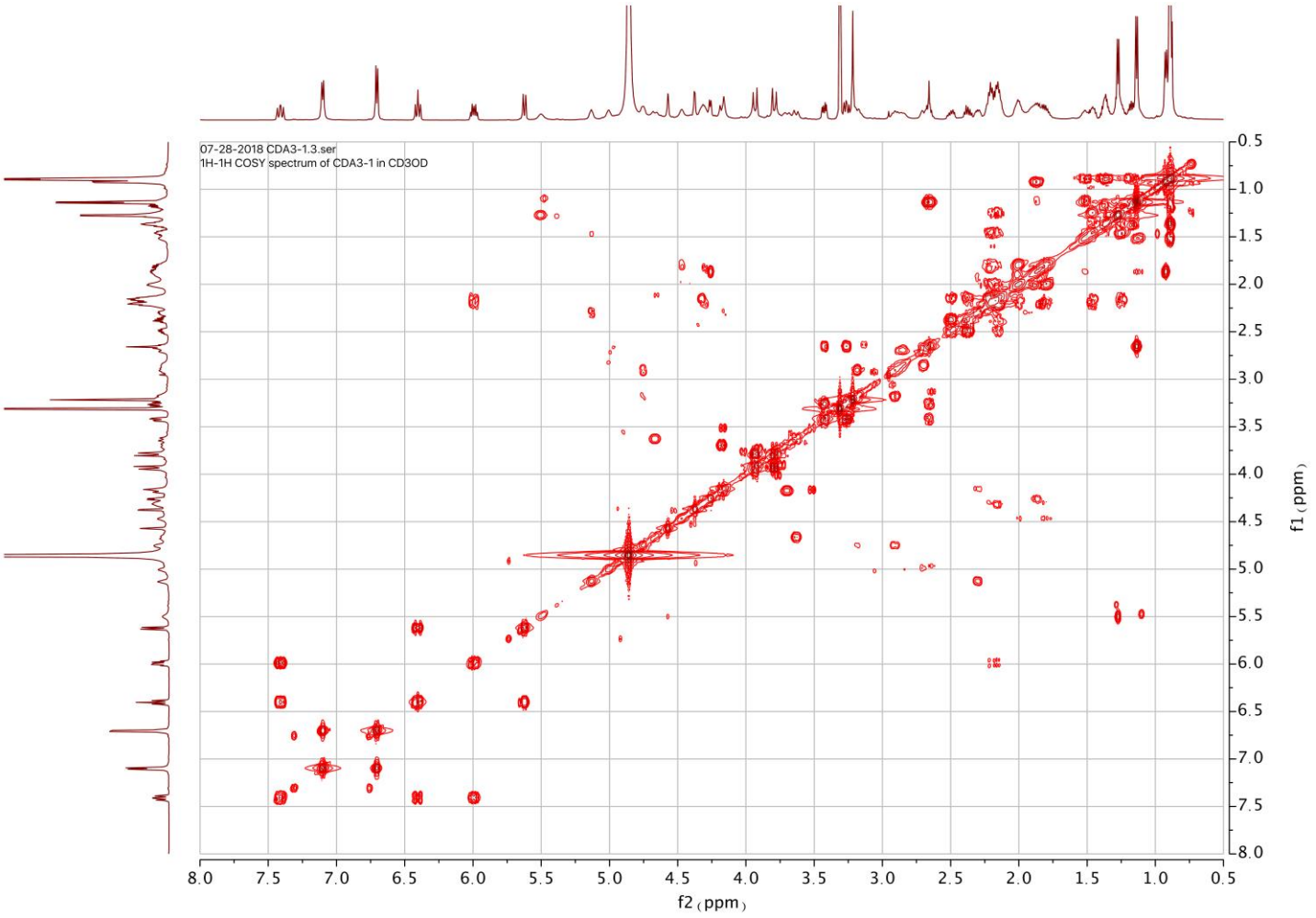

Figure S19. ^{1}H-^{1}H TOCSY NMR (600 MHz, CD_3OD) spectrum of cadaside A (**1**)

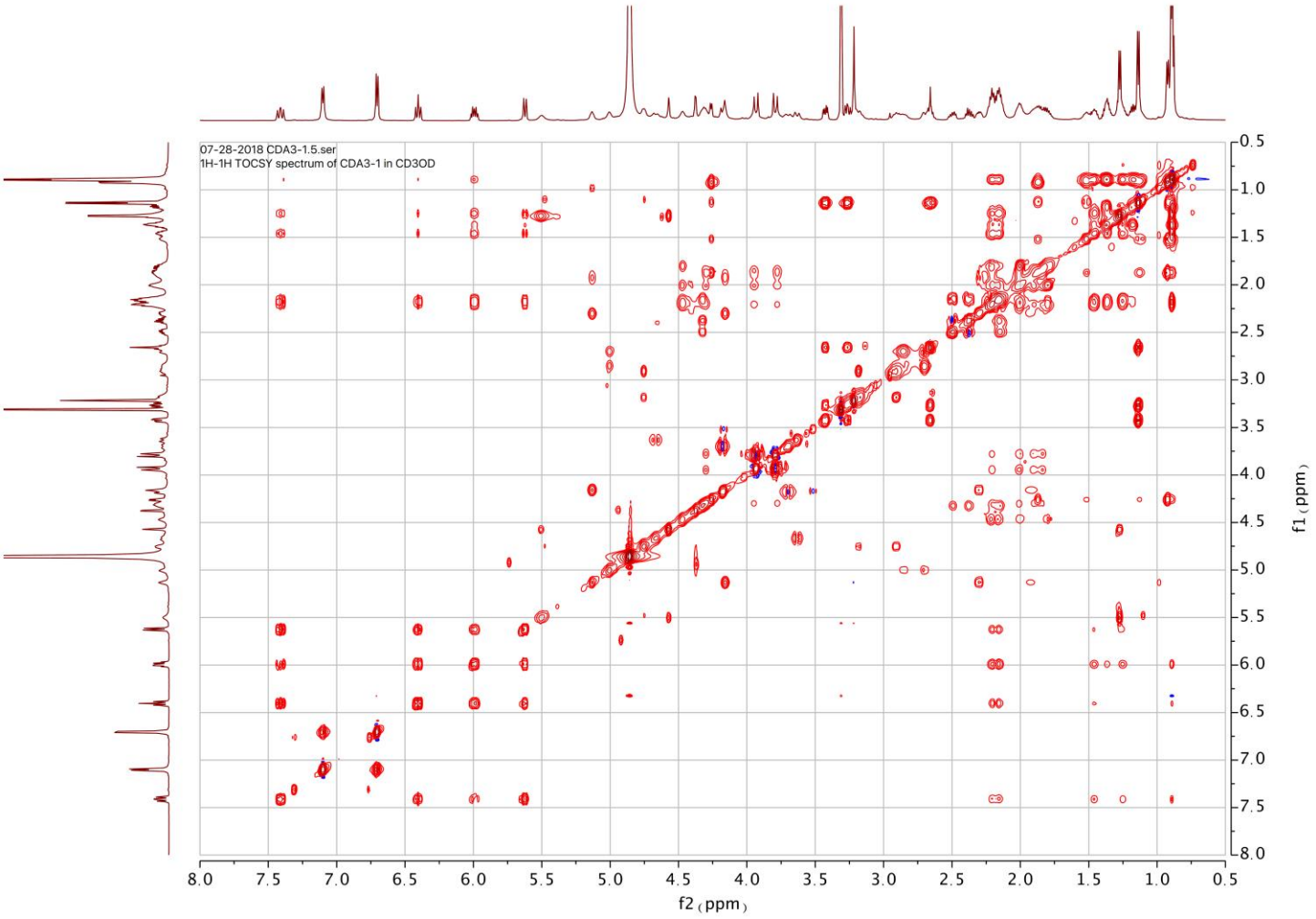

Figure S20. ^{1}H-^{13}C HSQC-TOCSY NMR (600 MHz, CD_3OD) spectrum of cadaside A (**1**)

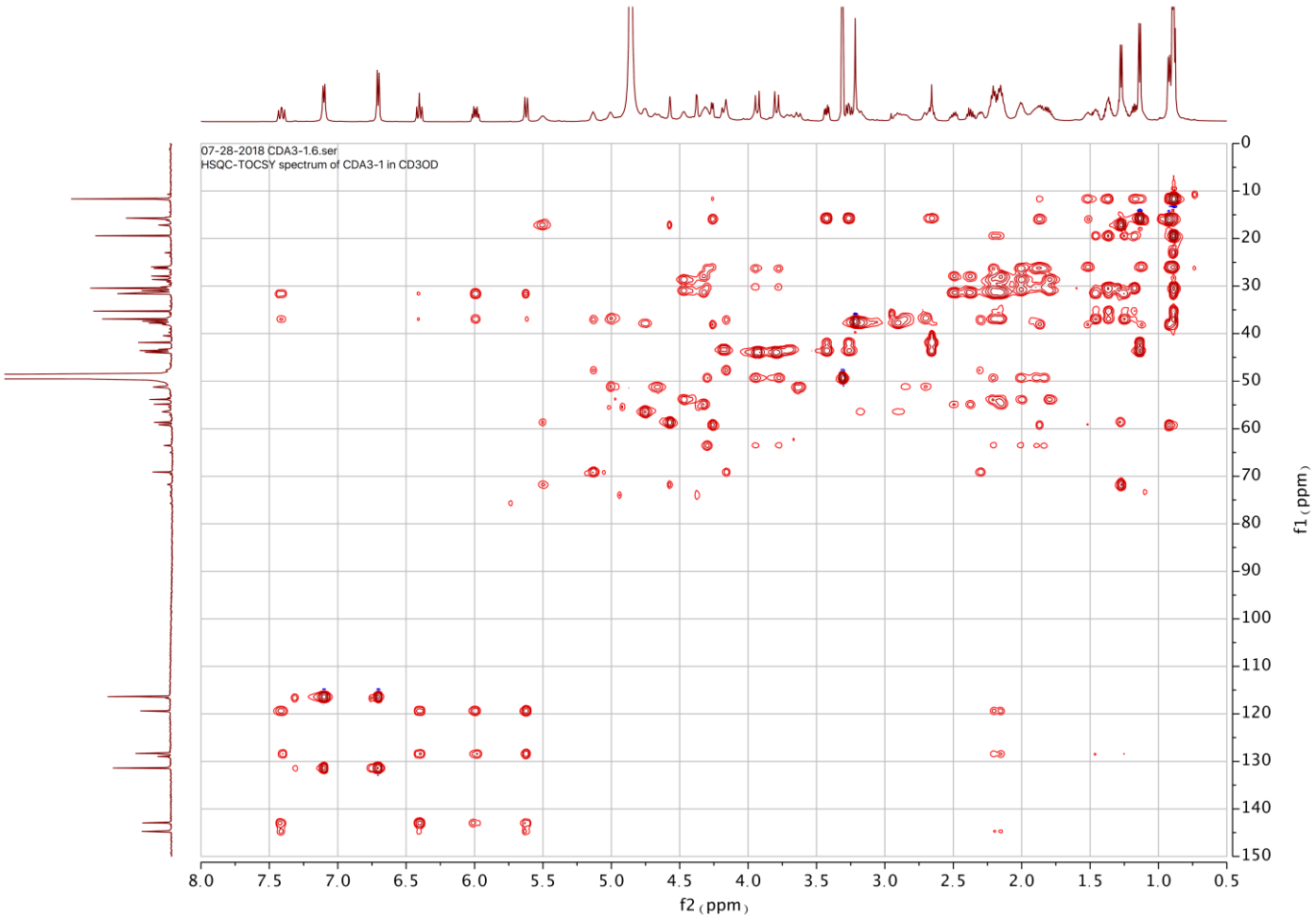

Figure S21. ^{1}H-^{1}H ROESY NMR (600 MHz, CD_3OD) spectrum of cadaside A (**1**)

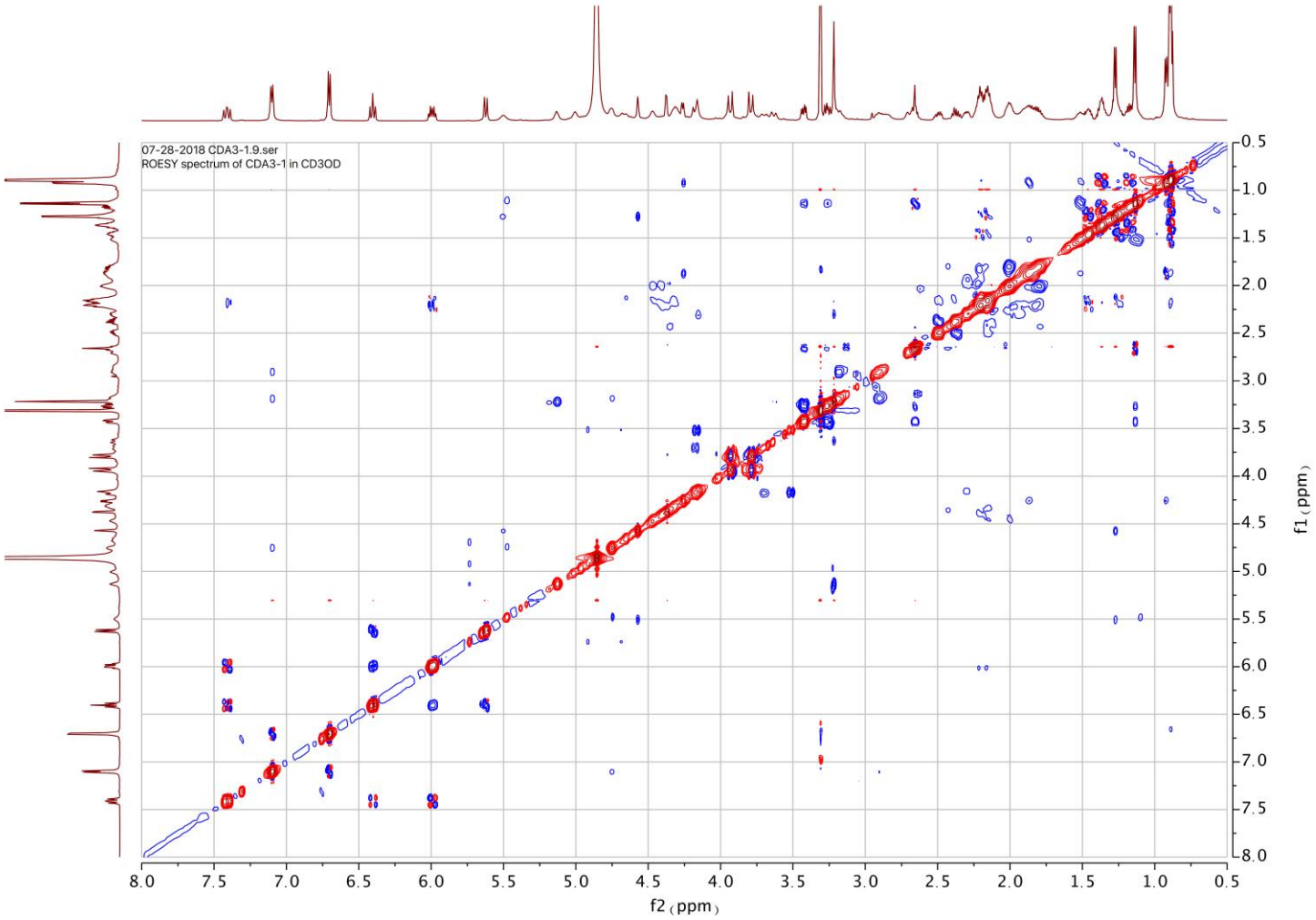

Figure S22. ^{1}H NMR (600 MHz, CD_3OD) and UV-vis spectra of cadaside B (**2**)

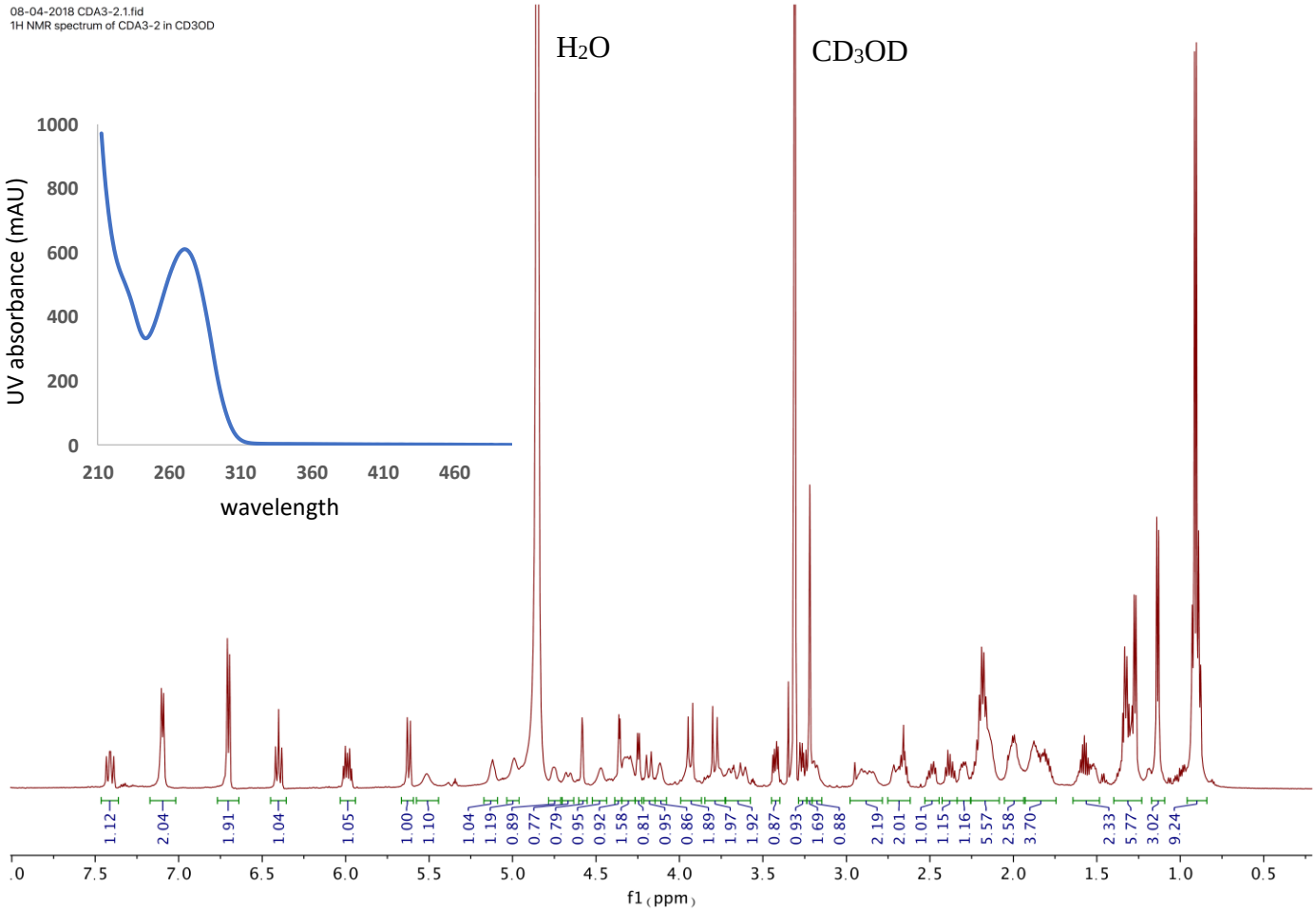

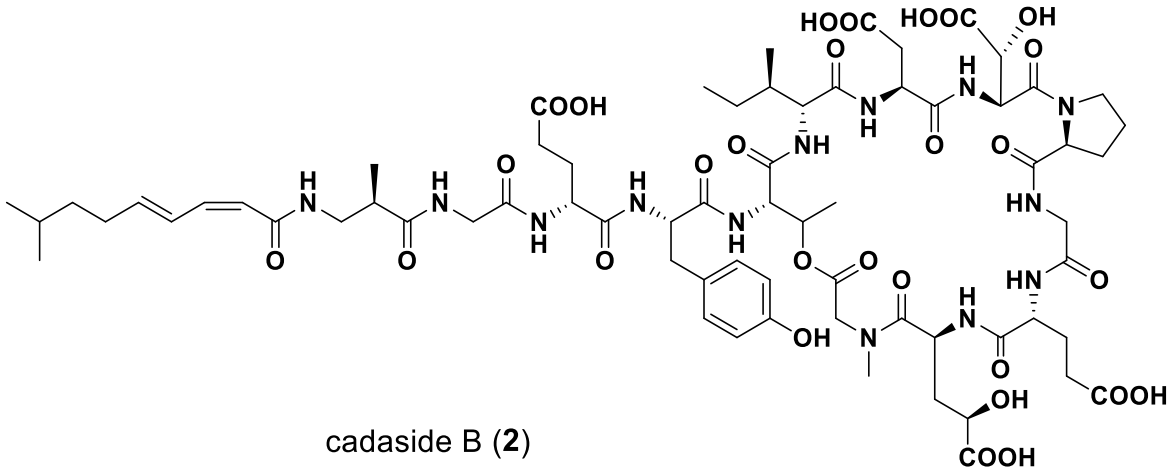

cadaside B (**2**)

Figure S23. ^{13}C NMR (150 MHz, CD_3OD) spectrum of cadaside B (**2**)

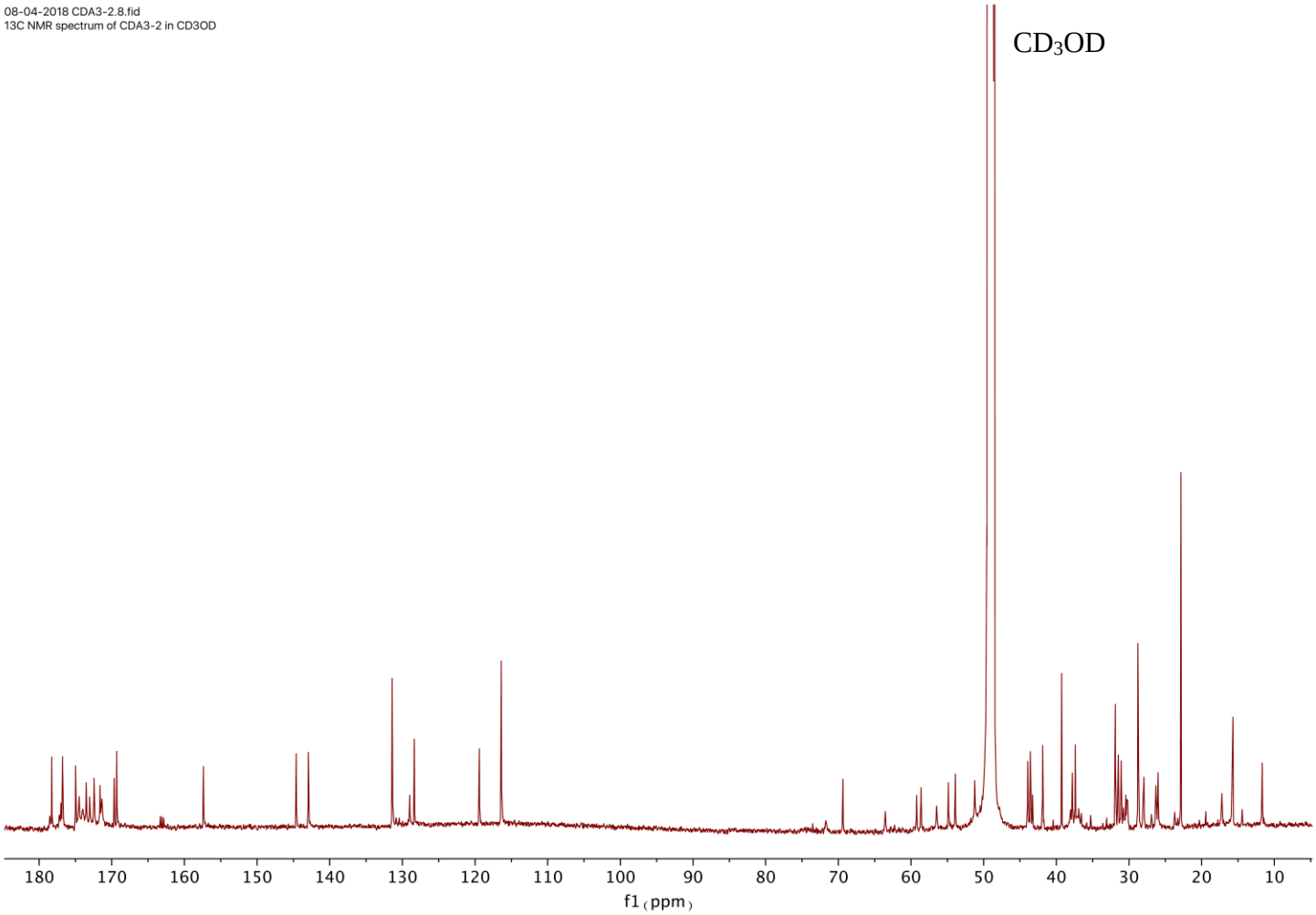

Figure S24. ^{1}H-^{13}C HSQC NMR (600 MHz, CD_3OD) spectrum of cadaside B (**2**)

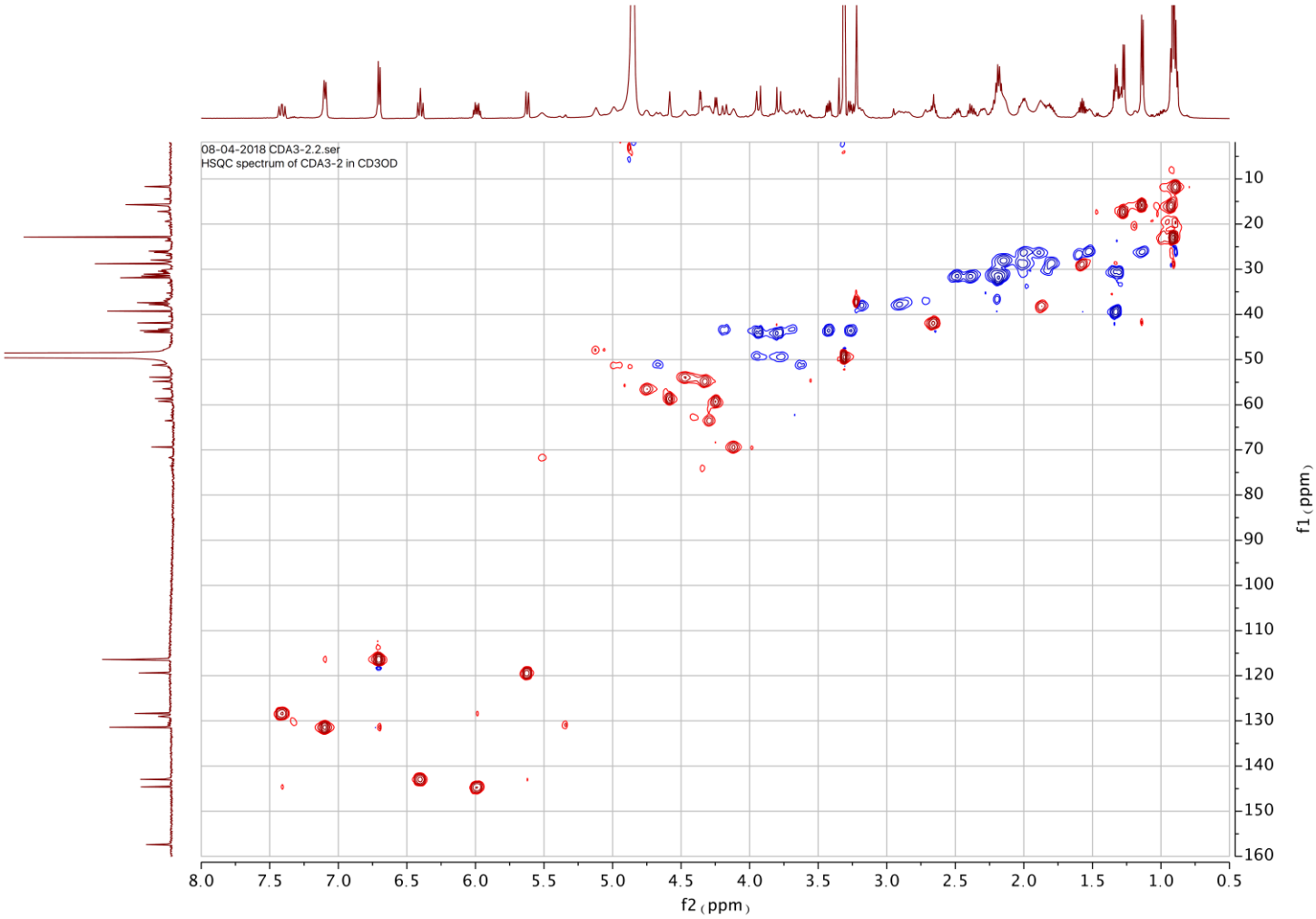

Figure S25. ^{1}H-^{13}C HMBC NMR (600 MHz, CD_3OD) spectrum of cadaside B (**2**)

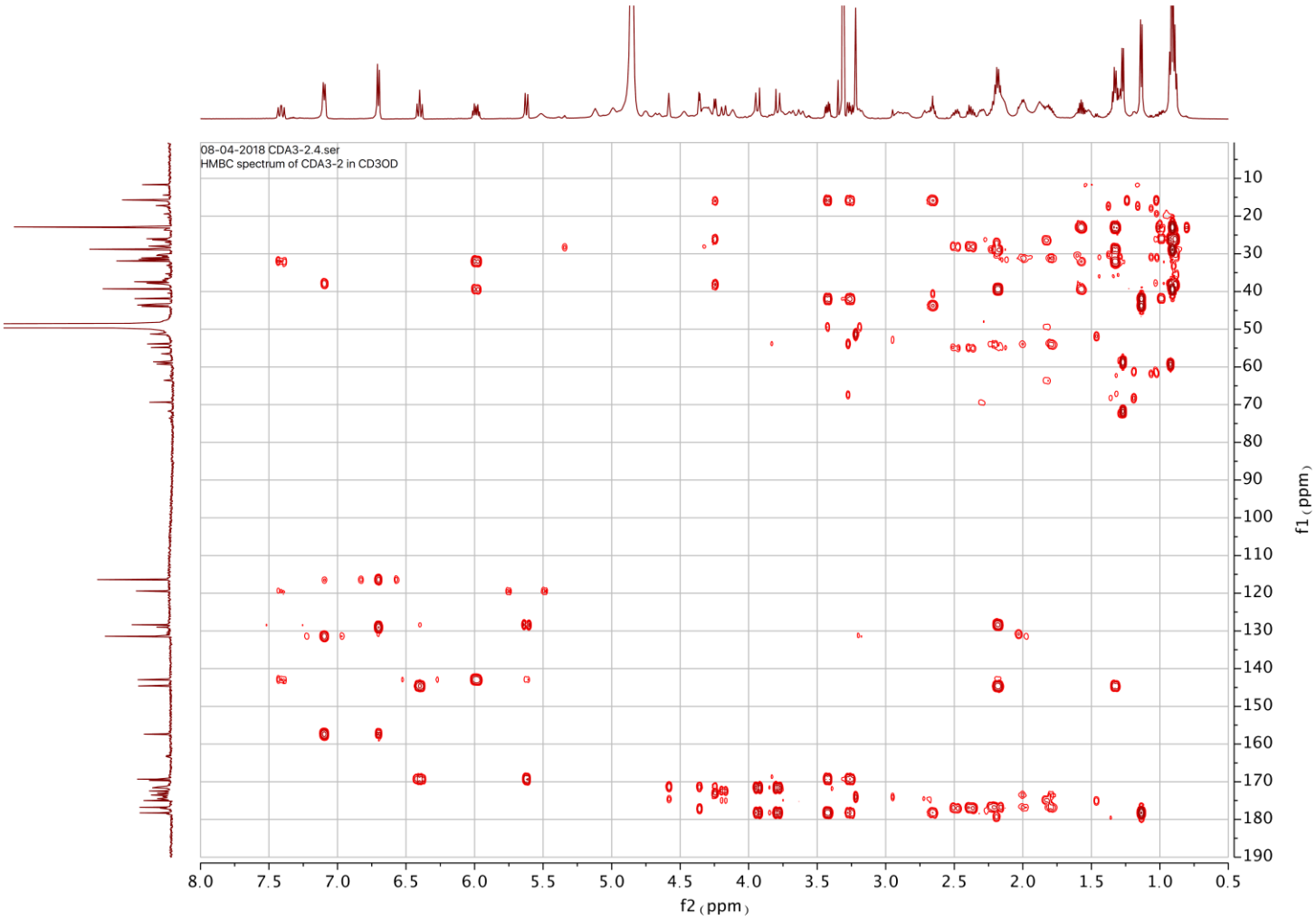

Figure S26. ^{1}H-^{1}H COSY NMR (600 MHz, CD_3OD) spectrum of cadaside B (**2**)

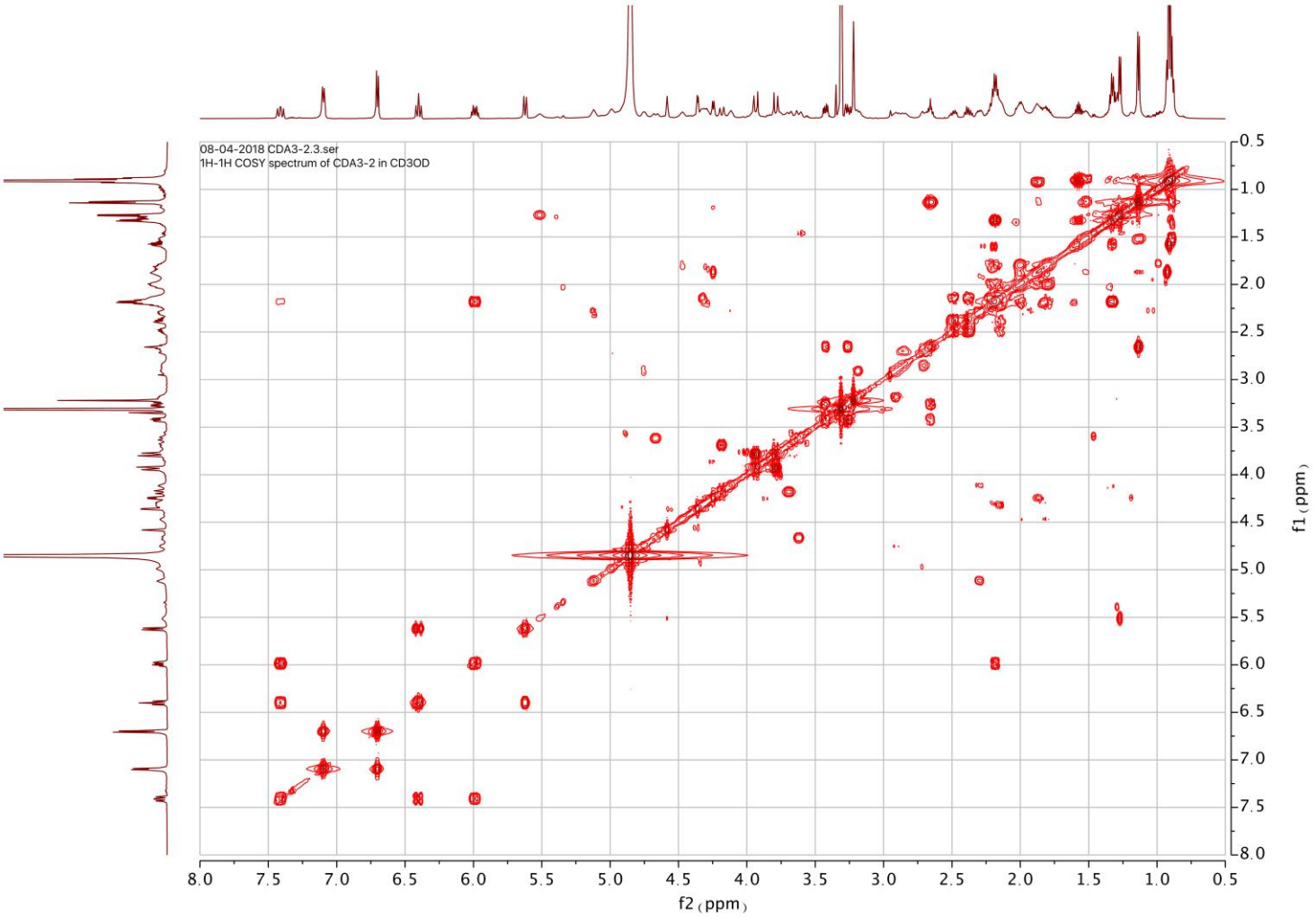

Figure S27. ^{1}H-^{1}H TOCSY NMR (600 MHz, CD_3OD) spectrum of cadaside B (**2**)

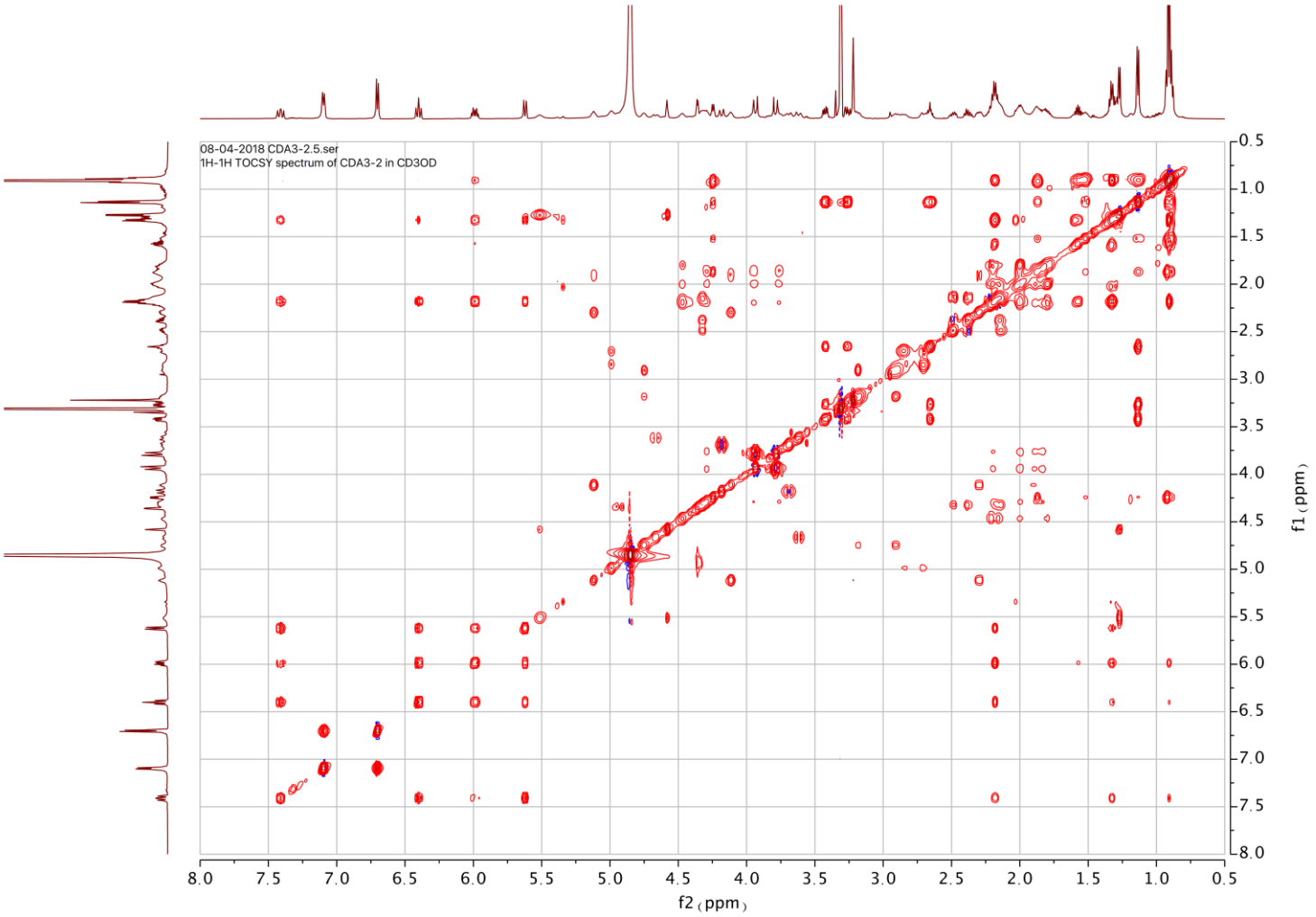

Figure S28. ^{1}H-^{13}C HSQC-TOCSY NMR (600 MHz, CD_3OD) spectrum of cadaside B (**2**)

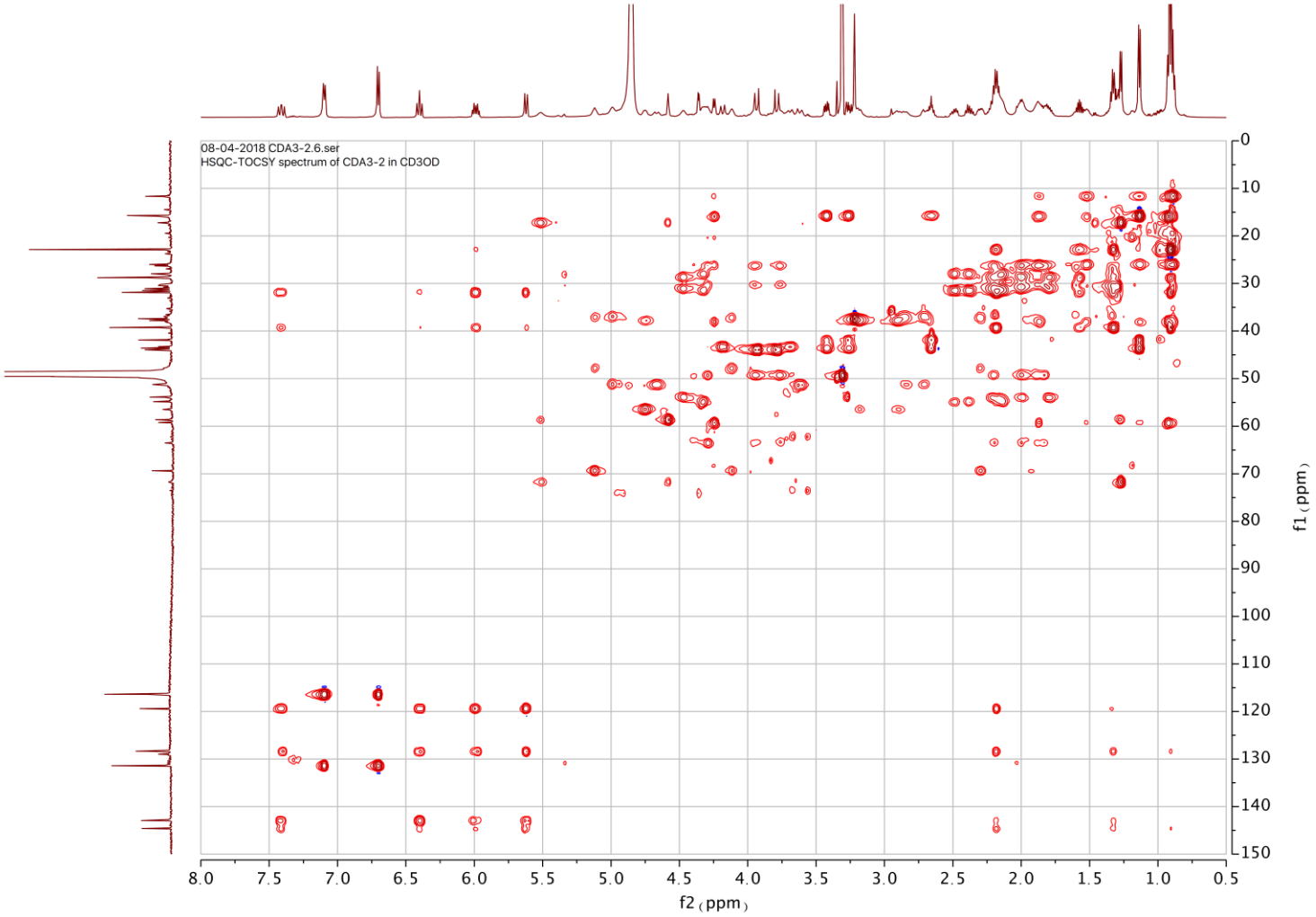

Figure S29. ^{1}H-^{1}H ROESY NMR (600 MHz, CD_3OD) spectrum of cadaside B (**2**)

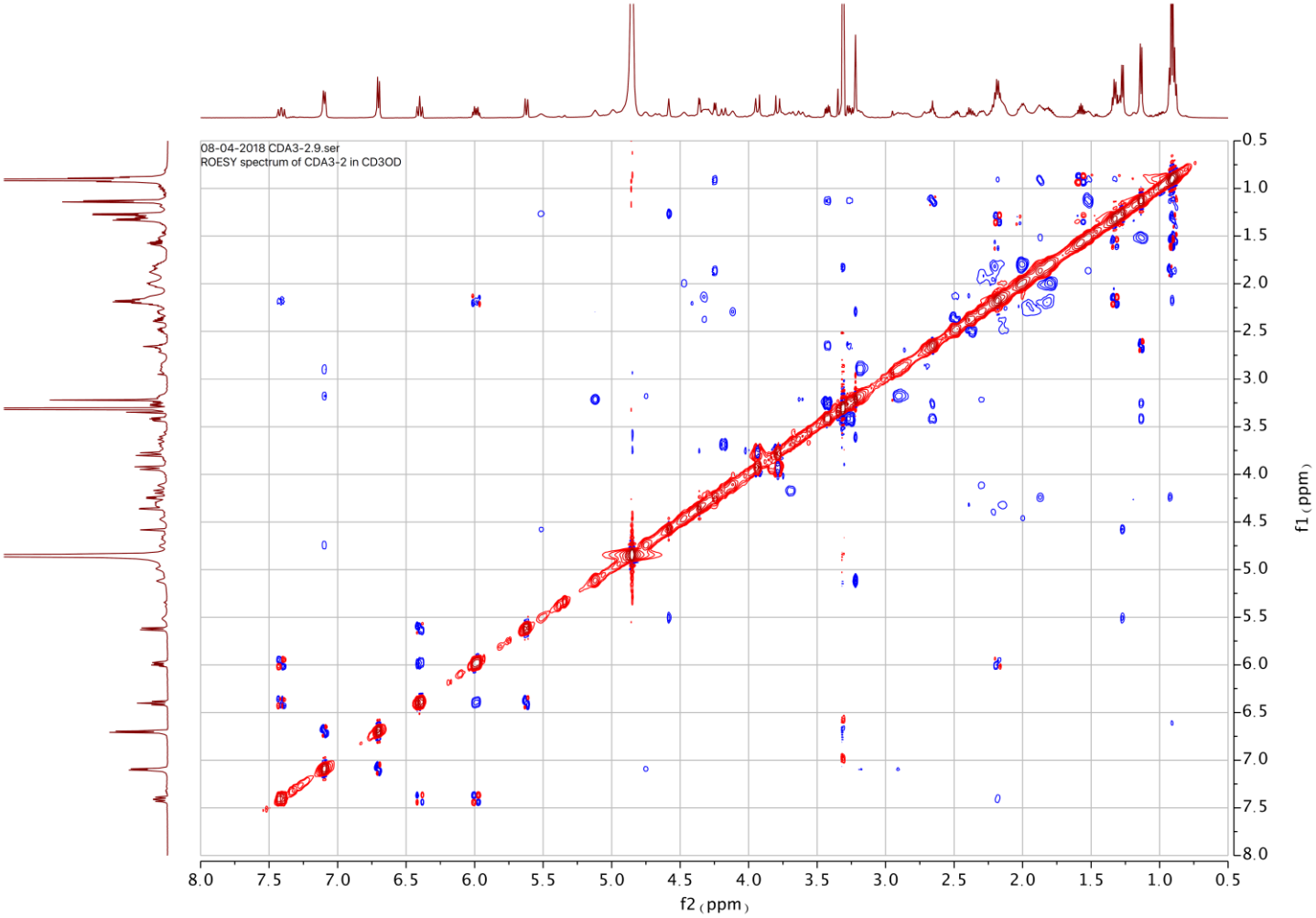

References

(1) Carmichael, J.; Degraff, W. G.; Gazdar, A. F.; Minna, J. D.; Mitchell, J. B. Evaluation of a Tetrazolium-Based of Semiautomated Colorimetrie Assay : Assessment of Chemosensitivity Testing. *Cancer Reserach* **1987**, *47*, 936–942.

(2) Schneider, T.; Gries, K.; Josten, M.; Wiedemann, I.; Pelzer, S.; Labischinski, H.; Sahl, H. G. The Lipopeptide Antibiotic Friulimicin B Inhibits Cell Wall Biosynthesis through Complex Formation with Bactoprenol Phosphate. *Antimicrob. Agents Chemother.* **2009**, *53* (4), 1610–1618.

(3) Schwyn, B.; Neilands, J. B. Universal Chemical Assay for the Detection and Determination of Siderophore. *Anal. Biochem.* **1987**, *160*, 47–56.

(4) Zhang, F.; Barns, K.; Hoffmann, F. M.; Braun, D. R.; Andes, D. R.; Bugni, T. S. Thalassosamide, a Siderophore Discovered from the Marine-Derived Bacterium *Thalassospira profundimaris*. *J. Nat. Prod.* **2017**, *80* (9), 2551–2555.

(5) Fujii, K.; Harada, K. I. A Nonempirical Method Using LC/MS for Determination of the Absolute Configuration of Constituent Amino Acids in a Peptide: Combination of Marfey's Method with Mass Spectrometry and Its Practical Application. *Anal. Chem.* **1997**, *69* (24), 5146–5151.

(6) Owen, J. G.; Reddy, B. V. B.; Ternei, M. A.; Charlop-Powers, Z.; Calle, P. Y.; Kim, J. H.; Brady, S. F. Mapping Gene Clusters within Arrayed Metagenomic Libraries to Expand the Structural Diversity of Biomedically Relevant Natural Products. *Proc. Natl. Acad. Sci.* **2013**, *110* (29), 11797–11802.

(7) Owen, J. G.; Charlop-Powers, Z.; Smith, A. G.; Ternei, M. A.; Calle, P. Y.; Reddy, B. V. B.; Montiel, D.; Brady, S. F. Multiplexed Metagenome Mining Using Short DNA Sequence Tags Facilitates Targeted Discovery of Epoxyketone Proteasome Inhibitors. *Proc. Natl. Acad. Sci.* **2015**, *112* (14), 4221–4226.

(8) Kreutzer, M. F.; Kage, H.; Nett, M. Structure and Biosynthetic Assembly of Cupriachelin, a Photoreactive Siderophore from the Bioplastic Producer *Cupriavidus Necator* H16. *J. Am. Chem. Soc.* **2012**, *134* (11), 5415–5422.

(9) Kohonen, T.; Curry, B.; Davies, F.; Phillips, P.; Evans, M. Mechanistic and Structural Basis of Stereospecific C_β-Hydroxylation in Calcium-Dependent Antibiotic, a Daptomycin-Type Lipopeptide. *ACS Chem. Biol.* **2007**, *2*, 187–196.

(10) Li, Q.; Qin, X.; Liu, J.; Gui, C.; Wang, B.; Li, J.; Ju, J. Deciphering the Biosynthetic Origin of L-allo-Isoleucine. *J. Am. Chem. Soc.* **2016**, *138* (1), 408–415.

(11) Fink, K.; Cline, R. E.; Henderson, R. B.; Fink, R. M. Metabolism of Thymine by Rat Liver i*n vitro*. *J. Biol. Chem.* **1956**, *221*, 425–433.

(12) van KUILENBURG, A. B. P.; STROOMER, A. E. M.; van LENTHE, H.; ABELING, N. G. G. M.; van GENNIP, A. H. New Insights in Dihydropyrimidine Dehydrogenase Deficiency: A Pivotal Role for Beta-Aminoisobutyric Acid? *Biochem. J.* **2004**, *379* (1), 119–124.

(13) Kim, S.; West, T. P. Pyrimidine Catabolism in *Pseudomonas aeruginosa*. *FEMS Microbiol Lett* **1991**, *61* (2–3), 175–179.